NASA/TM-2006-214274

Damage Tolerance Analysis of a Pressurized Liquid Oxygen Tank

Scott C. Forth, Stephen F. Harvin, Peyton B. Gregory, Brian H. Mason, Jon E. Thompson, and Eric K. Hoffman
Langley Research Center, Hampton, Virginia

February 2006

The NASA STI Program Office . . . in Profile

Since its founding, NASA has been dedicated to the advancement of aeronautics and space science. The NASA Scientific and Technical Information (STI) Program Office plays a key part in helping NASA maintain this important role.

The NASA STI Program Office is operated by Langley Research Center, the lead center for NASA's scientific and technical information. The NASA STI Program Office provides access to the NASA STI Database, the largest collection of aeronautical and space science STI in the world. The Program Office is also NASA's institutional mechanism for disseminating the results of its research and development activities. These results are published by NASA in the NASA STI Report Series, which includes the following report types:

- TECHNICAL PUBLICATION. Reports of completed research or a major significant phase of research that present the results of NASA programs and include extensive data or theoretical analysis. Includes compilations of significant scientific and technical data and information deemed to be of continuing reference value. NASA counterpart of peer-reviewed formal professional papers, but having less stringent limitations on manuscript length and extent of graphic presentations.

- TECHNICAL MEMORANDUM. Scientific and technical findings that are preliminary or of specialized interest, e.g., quick release reports, working papers, and bibliographies that contain minimal annotation. Does not contain extensive analysis.

- CONTRACTOR REPORT. Scientific and technical findings by NASA-sponsored contractors and grantees.

- CONFERENCE PUBLICATION. Collected papers from scientific and technical conferences, symposia, seminars, or other meetings sponsored or co-sponsored by NASA.

- SPECIAL PUBLICATION. Scientific, technical, or historical information from NASA programs, projects, and missions, often concerned with subjects having substantial public interest.

- TECHNICAL TRANSLATION. English-language translations of foreign scientific and technical material pertinent to NASA's mission.

Specialized services that complement the STI Program Office's diverse offerings include creating custom thesauri, building customized databases, organizing and publishing research results ... even providing videos.

For more information about the NASA STI Program Office, see the following:

- Access the NASA STI Program Home Page at ***http://www.sti.nasa.gov***

- E-mail your question via the Internet to help@sti.nasa.gov

- Fax your question to the NASA STI Help Desk at (301) 621-0134

- Phone the NASA STI Help Desk at (301) 621-0390

- Write to:
  NASA STI Help Desk
  NASA Center for AeroSpace Information
  7121 Standard Drive
  Hanover, MD 21076-1320

NASA/TM-2006-214274

Damage Tolerance Analysis of a Pressurized Liquid Oxygen Tank

Scott C. Forth, Stephen F. Harvin, Peyton B. Gregory, Brian H. Mason, Jon E. Thompson, and Eric K. Hoffman
Langley Research Center, Hampton, Virginia

National Aeronautics and
Space Administration

Langley Research Center
Hampton, Virginia 23681-2199

February 2006

Available from:

NASA Center for AeroSpace Information (CASI)
7121 Standard Drive
Hanover, MD 21076-1320
(301) 621-0390

National Technical Information Service (NTIS)
5285 Port Royal Road
Springfield, VA 22161-2171
(703) 605-6000

Abstract

A damage tolerance assessment was conducted of an 8,000 gallon pressurized Liquid Oxygen (LOX) tank. The LOX tank is constructed of a stainless steel pressure vessel enclosed by a thermal-insulating vacuum jacket. The vessel is pressurized to 2,250 psi with gaseous nitrogen resulting in both thermal and pressure stresses on the tank wall. Finite element analyses were performed on the tank to characterize the stresses from operation. Engineering material data was found from both the construction of the tank and the technical literature. An initial damage state was assumed based on records of a nondestructive inspection performed on the tank. The damage tolerance analyses were conducted using the NASGRO computer code. This paper contains the assumptions, and justifications, made for the input parameters to the damage tolerance analyses and the results of the damage tolerance analyses with a discussion on the operational safety of the LOX tank.

Introduction

A damage tolerance assessment was conducted of a pressurized LOX Tank. The LOX tank consists of a stainless steel pressure vessel enclosed by a thermal-insulating vacuum jacket. The subject LOX tank was utilized for rocket motor testing at Edwards Rocket Test Facility in California beginning in 1960 and concluding sometime prior to 1982, when the tank was first examined by NASA Langley personnel as surplus property. NASA Langley obtained the LOX tank during a project to upgrade the Eight-foot High Temperature Tunnel (8'HTT) in the mid 1980's. During operation, 85 pounds per second of cryogenic oxygen at 2250 psi is required to flow from the LOX tank to the facility. To achieve this flow rate and pressure, the LOX tank is pressurized to 2,250 psi with gaseous nitrogen for each operational cycle. A typical operational cycle has a two minute duration. The pressurization and subsequent depressurization of the tank produce both thermal and pressure stresses on the vessel wall. Finite element analyses were performed to characterize the stresses from operation. Engineering material data for the stainless steel was found from both the construction of the tank and the technical literature. An initial damage state needed for the damage tolerance analysis was assumed based on records of a nondestructive inspection performed on the tank. The damage tolerance analyses were then conducted using the NASGRO computer code [1]. This paper contains the assumptions, and justifications, made for the input parameters to the damage tolerance analyses, and a discussion of the results of the damage tolerance analyses.

LOX Tank Construction

The Liquid Oxygen Tank (LOX) was manufactured in 1959 by Yuba Consolidated Industries Inc., Southwest Welding and Manufacturing Division under contract to Rocketdyne, a Division of North American Aviation. The fabrication specifications are contained in the 1959 Rocketdyne Specification 218-7 with two addendums [2]. The tank and its vacuum jacket were required to meet the 1959 requirements of the ASME Boiler and Pressure Vessel Code, Sections VIII [3] and IX [4]. The fabrication of the pressure vessel was supervised by the Division of Industrial Safety for the State of California.

The tank is constructed of an inner stainless steel pressure vessel surrounded by a thermal insulating vacuum jacket. The stainless steel vessel was constructed using austenitic 347 stainless steel 4.73 inch thick plates welded together radially and circumferentially as shown in Figure 1. The top of the vessel is a 347 stainless steel 11 inch thick forged manway that was welded to the spherical vessel walls.

347 Stainless Steel

The AISI 300 series austenitic stainless steels were developed as corrosion-resistant alloys. These alloys posses excellent oxidation resistance and good high-temperature strength and creep resistance and are used extensively at cryogenic temperatures. They alloys

can only be hardened through cold work (non heat treatable).
The two main alloying elements in the austenitic stainless steels are chromium and nickel. Chromium (Cr) imparts corrosion and oxidation resistance while nickel gives the alloys its austenitic structure with its associated toughness and ductility. The base composition of these alloys is 18% chromium and 8% nickel. Varying the base composition and alloying with other elements creates grades with special characteristics. Type 347, which was used in the construction of the LOX run tank, has additions of columbium and tantalum added to stabilize the alloy for service in the 800°-1600°F range and to minimize carbide precipitation when welding for resistance to intergranular corrosion [5, 6]. The chemical composition and mechanical test requirements for the SA-240 type 347 are presented in ASME BPVC Section II [7].
At cryogenic service temperatures, all of the austenitic stainless steels have the good strength, ductility, and toughness. The typical mechanical properties of type 347 stainless steel at room temperature and -320°F are shown in Table 1 [3, 6, 8, 9].

Weldments

The shell plate segments and the forged manway and nozzles were welded to each other in a double-V groove weld (butt joint) configuration with full penetration back-up weld seams as shown in Figure 1. Weld process was shielded metal arc with a designated weld rod of 19-9Cb with 4% max C and 4-7% ferrite [10]. This is not a standard designation for welding rods but appears to be an AWS classification E347 weld rod. Based upon AWS A5.4 Specification for Stainless Steel Electrodes for Shielded Metal Arc Welding [11] (identical to ASME BPVC Section II, Part C SFA-5.4 [7]), the chemical composition and mechanical property requirements for the weld metal are defined.

Arc Welding

The austenitic stainless steels can be readily welded by almost all of the usual arc welding processes provided adequate steps are taken to prevent oxidation and carburization of the weldment. In arc welding, an electrical discharge arc consisting of a thermally ionized plasma gas is established between the welding electrode and the workpiece. The electrode may be a consumable and provide the filler metal for the weld deposit such as in shielded metal arc or it may be non-consumable and use a secondary filler metal such as in gas tungsten arc. In either case, the weld metal is protected from atmospheric oxidation by a fluxing slag or a chemically inert shielding gas. Commonly used arc welding processes include shielded metal arc, gas tungsten arc, gas metal arc, plasma arc, flux cored arc, and submerged arc welding [12, 13].

Filler Metal

Weld filler metal selection is based upon the service conditions and the properties that the weld metal has to display. In general, the deposited weld metal composition should nearly match the base metal composition when welding austenitic stainless steels to themselves [5, 13].

Carbide Precipitation

Precipitation of carbides at the grain boundaries can be a major problem in welding austenitic grade steels. Carbide precipitation is accelerated by exposure to temperatures within the sensitizing range (800 – 1600°F) and by increased time at temperature. When intergranular Cr carbides are precipitated, resistance to corrosion and stress corrosion decrease markedly. Decrease in corrosion resistance is due to the presence of Cr-rich carbides at the grain boundaries which results in the depletion of Cr in the adjacent matrix material. Sensitization may result from slow cooling from annealing temperatures, stress relieving or welding. Because annealing or stress-relieving requires the metal to be held at temperatures for a relatively long period of time, it is possible that the entire workpiece will be sensitized [5, 6, 12, 13]. Carbide precipitation can be prevented or corrected by any one of three means.

- Solution heat treat to put the carbides back into solution thus restoring the normal corrosion resistance. This is done by heating the weldment to a high temperature range (usually above 1850°F) and then cooling rapidly.
- Use extra low C grades (0.03% max C). These grades have sufficient immunity to carbide precipitation in the 800-1600°F temperature range to undergo normal welding or stress-relieving operations without impairment of the corrosion resistance.
- Use stabilized grades such as 321 or 347 which contain Ti, Cb, or Ta. These stabilizing elements have a greater affinity for C than does Cr and carbides of these stabilizing elements have minimum

susceptibility to precipitation at the grain boundaries.

Crack Susceptibility of Weldments

Welded joints in austenitic stainless steels are susceptible to hot cracking during solidification of the weld metal unless suitable precautions are taken. The degree and frequency of these cracks depend on the composition of the weld metal, the amount of stress developed in the weld as it cools, the thickness of the joint, ductility of the weld metal at high temperatures, and the presence of notches [5, 8, 13].

Weld metal with a fully austenitic microstructure is considerably more susceptible to cracking than weld metal with a duplex structure of ferrite in austenite. Generally, ferrite is beneficial when the welds are restrained, the joints are large, and when cracks can adversely affect service performance. Too much ferrite, however, may have detrimental affects on corrosion resistance in some environments and it also is detrimental to toughness in cryogenic service, and in high temperature service when it can transform to brittle sigma phase. Two-phase structures of austenite and ferrite exhibit the least cracking susceptibility when the ferrite is from 4-8%, with the remainder austenite. This is sufficient ferrite to break up the coarse grain structure of as-cast austenite and is effective way to prevent hot cracking. The compositions of most filler metals are adjusted by the manufacturers to ensure weld deposits that have the desired ferrite content. Type 347 weld metal is designed to resolidify with a small amount of ferrite to minimize cracking susceptibility.

Ferrite content can be measured on a relative scale by various magnetic instruments or can be calculated from the chemical composition of the weld deposits based upon constitutive diagrams such as Espy, DeLong, and WRC-1988 diagrams [5, 8, 11, 13]. The WRC-1988 diagram is considered the most accurate, and is the preferred diagram, in the welding industry for predicting the ferrite content for 300 series stainless steel weld metals.

Residual Stresses and Post-Weld Heat Treatment

During welding, as the molten weld metal pool begins to solidify and shrink, it begins to exert stresses on the on the surrounding weld metal and heat affected zones. When the weld metal first solidifies, it is hot and relatively weak and exerts little stresses. As it cools further, however, the stresses in the weld areas increase and eventually reach the yield point of the base metal and heat affected zone. In the case of multi-pass welds, the weld bead metal laid down first resists the shrinkage of subsequent built-up weld bead layers. As a result, the weld metal laid down first is strained in tension down the length (longitudinal direction) of the weld bead. For thick-plate butt joints, little shrinkage in the transverse direction is possible due to the constraint provided by the plate and the stiffening effect of the underlying weld bead. As a result, compressive stresses develop in the transverse direction to the weld bead. Figure 3 shows a schematic representation of the residual stress distribution in the welded butt joint [25].

When weldments are made in thick plate (> 1 in.), residual stresses can vary significantly through the plate thickness. Figure 4 shows the distribution of residual stresses in the three directions in the weld metal of a butt joint. Both the longitudinal and transverse stresses are tensile in areas near the surfaces of the weld while the residual stresses were primarily compressive below the surface.

Residual stresses can adversely affect the performance of welded structure. In tension, residual stresses may lead to high local stresses in weld regions of low toughness. This high local stress can initiate cracks that propagate by the applied working stresses that would not ordinarily propagate. Weldments with heavy sections may be susceptible to underbead cracking if the stress levels due to restraint are high. Weldments of the Cb stabilized grades such as type 347 are most susceptible to this type of cracking because of strain induced precipitation of Cb carbides [8, 14].

To relieve residual stresses and reduce the tendency for weld cracking, a post-weld stress relief is usually conducted. However, this may not be feasible depending upon the size of the welded structure. Stress relieving can be performed over a wide range of temperatures. The normal annealing temperature range for 347 steel is 1800° - 2000°F. While the primary purpose of the anneal is to obtain softness and high ductility, these steels may also be stress relieve annealed within the carbide precipitation range of 800° - 1500°F without increasing the susceptibility to intergranular corrosion. Recommended time at temperature ranges from about 1 hr/inch of section thickness at temperatures above 1200°F to 4 hr/ inch of section thickness at temperatures below 1200°F. For maximum ductility, the higher annealing temperature range of 1800° - 2000°F is recommended [5, 8, 14]. Based upon these annealing treatments for welds in austenitic stainless steels, the estimated percentage of residual stresses relieved at various temperatures are as follows:

1550° – 1650°F 85% stress relief

1000° – 1200°F 35% stress relief

To relieve the residual stresses in the weldments and reduce the tendency for weld cracking, the entire LOX run tank was post-weld stress relieved after fabrication. Indicated stress relieving at 1150°F for 44 hrs was required. A special note was added revising this heat treatment due to the 11 in.-thickness of the manway forging. The revised post-weld heat treatment for the LOX run tank was as follows:

Heat to 800°F and hold for 22 hours. Heat as rapidly as possible from 800°F to 1800°F and hold for 11 hours. Air quench. Based upon this stress relief and full annealing treatment, the estimated percentage of residual stresses relieved in the welds was 85 to 100 percent [8, 14].

Material and Weld Process Qualification

Weld qualification was conducted prior to fabrication to ensure that the actual weldments used in the construction of the LOX tank would have the required properties for the intended service conditions. Material and weld process qualification was conducted using weld procedure specification (WPS) and ASME BPVC, Section II, Parts A and C, Section VIII, Division 1 and Section IX [3, 4, 7, 11, 15]. In addition, a special material specification listed on Drawing No. D-8979 was used to qualify the materials and weld process used in the construction of the LOX tank for cryogenic service. This specification is as follows:

Special Certified Low temperature property tests, in addition to those required by the various codes, shall be required on each plate, forging, pipe, cap screws, and weld metal in the "as welded state" that is to be subjected to the working pressure stress of the inner vessel as follows:

Minimum requirements of metal in the annealed state at -300°F
Ultimate Tensile Strength: 150 ksi
Yield Strength: 35 ksi
Charpy Impact Strength: 30 ft-lbs
Elongation (In 2 Inches): 25 %
Reduction in Area: 50 %
Weld metal Charpy Impact Strength: 15 ft-lbs

Performance qualifying records for the 347 plate, forgings, and weld metal are shown in Tables 2-4. Tables 2 and 3 show the qualifying mechanical properties of the weld metal, shell segment plate, and forged flanges at -320°F while Table 4 shows the chemical analysis of the shell plate. No chemistries were listed for either the forged flanges or the weld metal. As per ASME BPVC Sec. VIII, Division 1 [3], no weld metal chemistries are required for qualifying welds for code approved base materials.

Fully austenitic stainless steel weld metals possess excellent toughness at cryogenic temperatures. To ensure freedom from brittle failure, ASME BPVC, Section VIII, Division 1 [3] requires weldments intended for cryogenic service to be qualified by Charpy V-notch testing. The criterion for acceptability is the attainment of a lateral expansion opposite of the notch of greater than 0.015 inches at -320°F. At the time of manufacture, the qualifying tests consisted of tensile and Charpy V-notch fracture toughness minimum values only. Based upon the above referenced test results, base material and weld metal mechanical properties are within code and special material specification and demonstrate sufficient strength, ductility, and fracture toughness for service at -320°F.

LOX Tank Repairs

The LOX tank was repaired on three separate occasions during it's service life. Additionally, NASA Langley modified the tank for use at the 8'HTT by welding plugs into 6 of the small nozzles (P1 thru P6). These repairs and modifications are documented below in order to provide a complete source of information regarding the repair history of the tank for future inspection and analysis of the LOX tank. The first weld repair of the LOX run tank occurred in 1965. The second and thrid repairs of the tank occurred in 1986 and 1991 respectively.

First Repair

There are records of a repair required on the tank in 1965. In an initial letter dated 12 January 1965 (attachment 1), it was stated that an inspection in the tank conducted on 5 January revealed cracks in the manway boss and nozzle P4. In a follow-up letter dated 14 January 1965 (attachment 2), a repair to Nozzle P4 was conducted, there is no information relative to why the repair was required. There is also no further mention of the manway boss crack. There is a hand written note on the 12 January note stating that the manway boss must have just been a surface scratch since it was never mentioned again. However, following the weld repair on P4, the tank was pneumatically pressure tested to 125% of operating pressure, then cleaned with acid, flushed, dried and re-inspected. The dye penetrant re-inspection revealed that nozzles P1 and P2 had cracks in the welds, and nozzle P3 with a surface scratch. Some additional analysis was conducted by Rocketdyne and on January 20, 1965 the decision was made to make the welds on all seven nozzles P1 thru P7 full penetration welds.

The weld repairs were completed and documented following proper procedures for an ASME code stamped vessel. The repair is documented in attachment 3, the U1A Report for the vessel after completing the repair. Following these repairs, no other indications were noted in this 1965 inspection. The qualifying weld procedure report for the weld repair is listed in Table 5 [16].

The Military Specification MIL E-22200 2A referred to in Table 5 is entitled Electrodes, Welding, Covered (Austenitic Chromium-Nickel Steel) [17] and applies to the shielded metal arc welding of austenitic stainless steels. For this repair weld, type E-308 ELC-16 electrodes were used. These electrodes are intended for general welding of 18Cr, 8Ni extra low carbon corrosion-resistant steels and are used where intergranular corrosion should be limited but where corrosive conditions are not the most severe. Although this welding electrode is not of the same composition as that of the 347 plate, it is permissible to use this electrode for 347 stainless steel. The recommended ferrite number shall be from 4 to 10 as determined by AWS A5.4 [11].

The reported values of 145 and 26 for the 1/8" and 165 and 26 for the 5/32" appear to the ultimate tensile strength (ksi) and Charpy V-notch (ft-lbs) for the weld metal at -320°F. The 1/8" and 5/32" indicate the weld rod diameter used. Due to the poor quality of the report, the description of these numbers cannot be determined. If we assume the same Special Certified low temperature property tests required at the time of manufacture, then the weld metal meets code for strength and fracture toughness at -320°F.

Based upon the FN determined from AWS A5.9 [11], the undiluted 308L weld metal had a FN of 9 based upon the nominal mid-range chemistry of the E308L weld rod. Weld metal dilution with the plate material will usually result in somewhat lower ferrite content than the undiluted weld metal depending upon the amount of dilution and the composition of the base metal. These values are within the recommended 4-9% ferrite range for reducing crack susceptibility in 347 weld metal [13].

No post-weld stress relief was used following the weld repair. Therefore, the residual stresses in the vicinity of the weld repair can be high and approach the yield point of the surrounding base metal and heat affected zone [14, 25].

Second Repair

A dye penetrant inspection was conducted after moving the tank from California to NASA Langley dated 28 July, 1986 (see attachment 4). The dye penetrant inspection report document states that the 8 circumferential welds, the 6 insert welds (with the seventh being inaccessible), the penetration at the entry hole, and all other penetrations of the shell were inspected. The liquid outlet at the bottom of the tank was listed as being inaccessible for inspection. The results from this inspection revealed two incomplete fusion indications in the top of the vessel, one incomplete fusion in the bottom of the vessel, and one crack-like indication at the bottom of the vessel. In a note, the inspector stated that the diffusers on the manifold were loose and that the interconnecting rods were worn. These items were addressed in subsequent repair work – however they did not require any work on the pressure shell itself.

On 5 December of 1986 a second dye penetrant inspection inside the tank was completed following light grinding of the four indications revealed in the earlier inspection. The inspection notes that the light grinding (less than 1/32") had removed the four indictations (see attachment 5). Following this inspection, a memo dated 16 January 1987 from the Fracture Mechanics Engineering Section stated that the LOX run tank had been judged safe for continued operation. Following this memo, the LOX tank installation into the 8'HTT began. The LOX run tank was not used for facility operation, including shake down testing, until July of 1992.

NASA records show that on 31 August, 1989 Chicago Bridge and Iron (CB&I) the Prime contractor for the 8'HTT modification project submitted the completed R-1 forms for welded modifications made inside the LOX run tank. The documentation for the weld modifications is covered in Section C of this report. The modifications consisted of welding plugs into nozzles P-1 through P-6. The plugs were used to seal off each of the shell penetrations which were not required for operation at the 8'HTT. The lower nozzle P7 is used for a differential pressure measurement which measures the height of the liquid in the run tank.

On 14 June 1990 thickness measurements were taken in the areas in which the four indications found in 1986 had been ground out. The measurements showed that wall thicknesses in the repair area were greater than 4.71 inches.

Following the NASA inpections and weld modifications completed by CB&I, a hydrostatic tank was conducted on the LOX tank. On 30 June 1990 the hydrostatic test report documents that the LOX run tank was hydrostatically tested to 1.5 times maximum operating pressure (1.5*2290 = 3435 psig). The hydrotest report document is shown in attachment 6. Following the successful hydrostatic test, the LOX run tank cleaning process (required for liquid oxygen service) was initiated.

Third Repair

The documentation then shows that as a check of the LOX cleaning, a portion of the nitrogen distribution manifold internal to the run tank was inspected and poor quality welds were found in the distribution manifold. In October of 1990, the weld review board met, and determined that the large diameter tee just inside the run tank should be cut, the distribution manifold lowered to the bottom of the tank, and weld repairs on this piping be completed. The weld review board meeting minutes are provided in attachement 11. The distribution manifold was repaired to meet ASME code requirements.

Records show (attachment 7) that also beginning in October of 1990, dye penetrant inspections inside the tank of all nozzles were conducted and documented in examination reports. These dye penetrant inspection reports are provided in attachment 8. In report number 109 dated 22 October 1990, six cracks were found around the perimeter of nozzle "V". It is not clear why these cracks were not found in the 1986 inspections. There were no operation cycles of the LOX tank over this period. The only pressurization occurred during the hydrostatic test. The process to grind out these cracks was initiated using dye penetrant inspections to insure that the entire crack had been ground out prior to beginning repair.

Dye penetrant inspection reports 110, 111, 112, 113, and 114 show that all other nozzles into the run tank were also inspected in December of 1990. Please recall that nozzles P1 through P7 had plugs welded into them by CB&I and had previously been inspected, therefore they were not re-inspected. Defects were found in nozzles M, A. No defects were found in nozzles N, D, or P. The defects found in nozzles M and A were removed via grinding and no weld repair was required. The records show that after grinding, each nozzle was re-inspected and no indications were found.

For the weld repair around nozzle V, all repair work was conducted and documented properly and inspected by the National Board. The welding procedure is documented on 28 November 1990 and the completed weld repair is and documented in a Report of Welded Repair submitted on 1 May 1991. The dye penetrant inspection record number 109 shows that following the completed repair, nozzle V was dye penetrant inspected on 1 February 1991 and no defects were found. The lox run tank oxygen cleaning resumed and the tank was cleaned for oxygen service. The LOX run tank was certified clean on 29 February 1992.

The welding procedure for the repair of the cracks found in the weld surrounding nozzle "V" and for welding the plugs into nozzles P-1 through P-6 was gas tungsten arc welding (GTAW) using bare ER316L stainless steel welding electrodes. Although this weld process differs from that used in the manufacture (shielded metal arc welding), it is an acceptable alternative.

Filler metal ER316L has a nominal composition (wt. %) of 19Cr, 12.5NI and 2.5Mo with low carbon (0.03 % max). The low carbon in this filler metal reduces the possibility of intergranular chromium carbide precipitation and thereby increases the resistance to intergranular corrosion without the use of stabilizers such as columbium or titanium. The molybdenum provides enhanced creep resistance at elevated temperatures. The filler metal is used primarily for welding low-carbon molybdenum-bearing austenitic alloys. The ER316L filler metal is often used for service at cryogenic temperatures because of its high toughness due to its high Ni content and it does not crack at very low ferrite levels [13, 18].

The weld metal tensile strength at ambient temperature averaged 83 ksi while the Charpy-V notch fracture toughness at -320°F averaged 31 ft-lbs with a lateral expansion opposite the notch opening exceeding the 0.015 inch minimum allowable threshold. The reported 10% shear fracture area is a qualitative measurement that estimates the relative amount of shear fracture versus that of cleavage or brittle fracture. Lateral expansion is also used to indicate the relative amount of ductile tearing during fracture. Lateral expansion is reported as the increase in width of the broken specimen over the unbroken specimen width. A brittle specimen will not have significant tearing at the sides and the width of the specimen will be very close to that of the unbroken specimen. A tough specimen will have extensive shear lips that deform the specimen into the width direction.

Based upon the FN determined from AWS A5.9 [18], the undiluted 316L weld metal has a FN of 8 based upon the nominal mid-range chemistry of the ER316L weld rod. Further dilution between the 347 plate metal and the 316L weld metal would somewhat lower the ferrite content. This value is within the recommended 4-8 percent ferrite range for reducing crack susceptibility in the weld metal [13]. The weld repair qualification records for the tensile and Charpy V-notch of the 316L weld metal meet the current requirements for strength, ductility, and fracture toughness for -320°F service.

No post-weld stress relief was used following the weld repair surrounding nozzle V (Figure 5). Therefore, the residual stresses in the vicinity of the weld repair can be high and approach the yield point of the surrounding base metal and heat affected zone [14, 25].

LOX Tank Stresses

The LOX tank is an 8,000 gallon capacity, 2,290 maximum operating pressure, vacuum jacketed, vessel. The LOX tank is maintained in a cryogenic condition at all times, full or at least partially full of liquid oxygen. The run tank sits at atmospheric pressure at all times except during a facility run. The LOX tank is pressurized during operation using gaseous nitrogen. The gaseous nitrogen enters at the top of the tank at 520 degrees Rankine (60 degrees Fahrenheit). During operation, a pressure control valve is used to ramp the run tank pressure up to 2,250 psig, then hold this pressure level for the duration of the run, typically one minute. Immediately after each run, the LOX tank nitrogen gas is vented and the tank returns to atmospheric pressure. A plot showing the pressurization cycle for a typical run is shown in the attached Figure 6.

Pressure Stresses

Two finite element models were constructed to model the pressure stresses in the LOX tank during operation. The first model presented was constructed using Pro Engineer [19] and analyzed using Mechanica [20]. The second model was constructed using Patran [21] and analyzed using Abaqus [22]. The details of each analysis are presented separately followed by a discussion of the modeling results.

Mechanica Model

Three structural Finite Element Models were developed using Pro Engineer. For the first two models, top and bottom, a spherical coordinate system was used (R, θ, ϕ). The constraints along the shell boundary are θ and ϕ and the models have constant pressures on the inside surfaces of the spherical shell and the penetrations. The third model, which is a slice of the shell, uses a cylindrical coordinate system (R, θ, Z) with constraints of θ along the shell boundary and a vertical constraint Z on the lower surface of the support bracket. The third model uses a variable pressure that is a function of the height to obtain a vertical reaction due to the weight of the LOX and shell. A negative pressure is applied to the surface where a pipe would connect to a penetration on the outside to account for the open area of the penetration. Figure 7 is a solid model representation of the Pro-Engineer model used to develop the Mechanica finite element models with the nozzles labeled.
The top, side and bottom of the tank were analyzed with refined models to evaluate the stress concentrations from the nozzles and the support brackets on the side of the tank during pressurization. The maximum stress of 57.7 ksi was found to be at the interior of Nozzle N during the pressurization of the tank, as shown in Figure 8, and is the only one of the three models shown herein.

Abaqus Model

Three finite element models of varying discretization were created to analyze the LOX tank. Models with a coarse mesh having 11,062 8-node hexahedron elements, a medium mesh having 11,062 20-node hexahedron elements and a fine mesh having 37,388 20-node hexahedron elements are shown in Figure 9a-c, respectively. In Figure 9 the nozzles are blue, the welds between the nozzles and the tank are red, the section of the tank from the original model is green, and the rest of the tank hemisphere is yellow.
The von Mises equivalent stress distribution near Nozzles V, D and N is shown in Figure 10. The maximum von Mises stress was located at the same location (near Nozzle N and shown in the figures) in all cases and had a value of 40.86 ksi, 45.24 ksi and 45.66 ksi for the Coarse, Medium and Fine mesh models, respectively. The difference between the values obtained for the Medium and Fine mesh models is less than 1%, indicating that the discretization is converged.

Discussion of Pressure Stress Models

The maximum value of von Mises stress (45.66 ksi) predicted by the Abaqus model is lower than the maximum value (57.7 ksi) predicted by the Mechanica model. This difference is due to several factors including geometric differences in the two models, as shown in Figure 11. In Figure 11, a cross-section of the tank near the manhole cover is shown along with the design drawing from which it was created. The solid and dashed lines represent the local configuration of the Mechanica and Abaqus models, respectively. This geometry difference causes a shift in the location of the corner at which the curved tank wall and the flat surface of the manhole cap intersect. In the Mechanica model, this corner intersects the edge of the hole of Nozzle N, as shown in Figure 12. In the Abaqus model as in the design drawings, this corner does not intersect the edge of the hole of Nozzle N, as shown in Figure 12. In physical structures, stress concentrations occur at the edges of holes and at the corners. Because the hole and the corner overlap in the Mechanica model, both stress concentrations occur at the same location resulting in a magnified maximum stress. In

the Abaqus model, the stress concentrations do not occur at the same place and the maximum stress is not magnified.

Thermal Stresses

The thermal stresses are calculated by computing a conservative temperature profile. An analysis was conducted in which the nitrogen mass flow rate into the LOX tank during an operational cycle was estimated from the depressurization rate of the dedicated nitrogen field providing the pressurization gas. The mass flow rate of nitrogen was used to obtain the pipe flow Reynolds number, which was in turn used to estimate the convective heat transfer coefficient on the inside surface of nozzle "V" (the nitrogen inflow nozzle). For the transient thermal analysis it was assumed that the entire structure was initially at the temperature of the liquid oxygen (-300 °F = 160 °R), while the surface of the nitrogen inlet nozzle (nozzle V) was convectively heated by the gaseous nitrogen flowing through nozzle "V". A summary of the calculation method used for the transient heat transfer analysis is on final in the document archives at the 8'HTT. From this information,transient temperature profiles were calculated. The thermal stresses were calculated using finite element models developed in Patran [21]. Nastran [23] was used to compute the resulting thermal stresses.

Three thermal stress finite element models were developed. The structural models were not used because many more elements are needed through the thickness of the tank and nozzle walls to capture the thermal stresses. The model was developed in a cylindrical coordinate system (R, θ, Z) and is wedge shaped with symmetry in the θ direction. The heat transfer coeffient versus run time is shown on Figure 13. The heat transfer coefficient was calculated using an equation from Kays and Crawford for a circular tube with fully developed velocity and temperature profiles, constant heat rate and Reynolds's number < 10^5 [24]. The physics of thermal stress analysis is complicated because the thermal profile is not fully developed, the Reynolds's number is one to two orders of magnitude larger, the geometry has been simplified and backside natural convection and radiation have been ignored. In order to insure that the analysis was still conservative, a factor of ten was applied to the heat transfer coefficient. The modified values of the heat transfer coefficient used in the analysis are shown on Figure 14.

For the inside surface of the nozzle V, the highest thermal stresses occured at a time of 62 seconds. The resulting temperature profile is shown in Figure 15. The thermal stresses are shown in Figure 16. The maximum thermal von Mises stress is 107 ksi. For the backside of the nozzle on the inside of the shell, the highest thermal stresses occur at a time of 245 seconds. The resulting temperature profile is shown in Figure 17. The thermal stresses are shown on Figure 18. The maximum thermal von Mises stress in this region is 33 ksi.

Damage Tolerance Model

The area of interest for a damage tolerance analysis is the top of the spherical LOX tank where a forged cover and three nozzles are welded to the tank. When pressurized for operation, the top of the tank witnesses the highest pressure and thermal stresses. The pressure stresses are high in this region because of the nozzle geometric details. The thermal stresses are highest because of the introduction of gaseous nitrogen to pressurize the tank through Nozzle V.

The input to the damage tolerance model is broken down into separate sections on geometry, residual stresses, applied stresses, initial crack size, and material properties.

Geometric Input

The forged top of the tank is nearly flat, so the contributions of out-of-plane cracking will be minimized, such that the simplification of the crack growth model to a think-plate solution is reasonable (and 19). The geometric model was constructed to simulate cracking between the two Nozzles V and N (Figures 19 and 20). The geometric dimensions (inches) used are: t = 4.73, W = 7.0, a_i = 0.5, and a/c = 1.0.

Stress Distribution

Three distinct stress distributions affect the damage tolerance analyses at the top portion of the LOX tank. The LOX tank is pressurized with room-temperature gaseous nitrogen during operation leading to pressure and thermal stresses. The construction and subsequent repair of the LOX tank left residual stress fields around the welments. In the damage tolerance analysis, the pressure (Figures 8, 10 and 21) and thermal stresses (Figures 16, 18 and 22) are superimposed with the residual stresses from construction (Figure 2) and repair welding (Figure 3) where the x and y coordinates are defined in Figure 23.

Pressure stress

The pressure stresses were computed using Mechanica and Abaqus based on the pressure cycle shown in Figure 6. The highest pressure stresses on the tank were computed using the Mechanica model and were located in the vicinity of Nozzles N and V as shown in Figure 8. Therefore, the pressure stresses used in the damage tolerance analyses are:

Principal pressure stresses are 16 - 22 ksi between the Nozzles (Figure 21)

Assume tank stresses are approximately zero between runs, *i.e.* load ratio, R = 0 (Figure 6)

Pressure at run = 2250 psi

Pressure between runs = 5 psi

Thermal stress

Nozzle V is the nitrogen fill nozzle for pressurizing the tank and therefore experiences the highest thermal stresses. A thermal stress analysis was performed using convective heat transfer into the nozzle based on the thermal cycle the tank undergoes, as shown in Figure 14. The thermal stresses used in the damage tolerance analyses are:

Local thermal stresses are a constant 3.74 ksi between Nozzles V and N (Figure 22)

Residual stress

The construction of the LOX tank involved welding several sections together to form the sphere and then welding a forged cover and several nozzles to the top of the tank (Figure 1). The welds are all butt-welds as shown in Figure 1. It is assumed that the residual stresses from the initial construction of the tank have the profile of tension at the tank surfaces and compression in the interior (shown in Figures 2 and 3) based on information presented in the Welding Handbook [12-14] and ASTM STP 776 [25].

The tank was repaired in 1990 as reported in contract 18367C [26]. The inspection report details the weld repairs around Nozzle V as shown in Figure 5. The repair welds were not heat treated, and based on ASTM STP 776 [25] the residual stresses are tensile along the weld-line and their variation along the length (x-direction) is presented in the bottom part of Figure 23. The crack growth analyses are performed by adding the residual stresses as steady stresses (increasing the stress ratio only), since this is an accurate representation of how the residual stresses would impact crack growth.

Assume residual stresses from manufacture are 15% of room temperature yield

σ_{res} = 5.5 ksi

Profile is tension at the surfaces and compression at the depth (Figure 23)

Assume residual stresses from the weld repair to be equal to room temperature yield

σ_{res} = 35 ksi

Profile is tension at the weld repair and transitions linearly to zero stress at a dimension of ¾ of the thickness (3.55 inches) in both the thickness and width directions.

Initial Crack Size

The initial crack size for the damage tolerance analysis is based on the method of NDI used in the inspection report. For the repair procedure, dye penetrant was used and based on NASA STD-5009 [27] an initial corner crack of 0.1 inches in radius should be used for the damage tolerance analyses. Additionally, in this case, a dye penetrant inspection revealed a ½ inch crack in the weldment of Nozzle V (Figure 5). The crack was ground out and a weld repair was performed. A subsequent penetrant inspection did not reveal any indications at the weld repair. For this analysis, it was presumed that the repair did NOT remove the crack from the LOX tank. Therefore, the initial crack sizes chosen were 0.5 and 0.1 inch radius corner cracks initiating at the weld repair.

Material Properties

The LOX tank is primarily constructed of 4.73 inch thick 347 Stainless Steel plate welded together using 347 SS wire. The top section, where the nozzles are located, is 10.25 inch thick 347 SS forging welded to the nozzles and sphere as shown in Figure 1. All crack growth considered in the damage tolerance analysis is contained within the weld connecting the forging to the sphere. Therefore, the material properties used in the analysis are representative of 347 Stainless Steel weldments at a temperature of -320 F. Table 2 contains the tensile data was generated during the initial qualification of the tank [2], data for welds in this alloy was found in the literature [28], and data was generated for the repair welds (Table 3) . Fracture toughness was calculated using Rolfe, Novak and Barson [29] from Charpy data, such that

$$K_{Ic} = \sigma_{YS}\sqrt{5\left(\frac{C_{VN}}{\sigma_{YS}} - 0.05\right)} \qquad (1)$$

where σ_{YS} is the yield stress at temperature for the material condition (parent or weld). The Stainless Steel 347 has a yield stress (parent material) of 36.5 ksi

at room temperature and 75.1 ksi at -325F (Tables 1, 2 and 3). The properties used in the analysis are the average yield and ultimate stresses from the construction weldment and the average fracture toughness of the repair weld data. The fracture toughness values calculated from the Charpy data are similar to those found in the NASGRO database [1] and ASME code [3] for other austenitic stainless steels. Therefore, the material properties input into NASGRO for the damage tolerance analyses are:

347 Stainless Steel Fracture Toughness and Yield/Ultimate data for weldments
- Yield = 48.9 ksi
- Ultimate = 172.2 ksi
- Fracture toughness, K_{IC} = 83.0 ksi $in^{1/2}$
- Thickness dependent fracture toughness, K_{Ie} = 116.0 ksi $in^{1/2}$

304 Stainless Steel da/dN curve fit (Fits the high R cryo data and bounds weld data), units are US Costumary (Figure 24)
- NASGRO Coefficients: UTS = 172.2, Yield = 48.9, K1e = 116, K1c = 83, Ak = 0.75, Bk = 0.5, a0 = 0.0015, Kth(s)/Kth(l) = 0.2, C = $6x10^{-10}$, n = 3.0, p = 0.25, q = 0.25, DK1 = 1.84, Cth = 0.63, Cth- = 0.1, Alpha = 2.5, Smax/Flow = 0.3, Cth = 0 throughout.

Damage Tolerance Analyses

The crack growth analyses were performed using NASGRO 4.22. The geometry chosen was CC09; the material properties were for 304 Stainless Steel at room temperature with modified values for yield stress, ultimate stress, K_{IC} and K_{Ie}; a nonlinear stress profile in both the x (thickness) and y (length) directions were developed to include pressure, thermal and residual stresses; and a corner crack of 0.5 inches in radius that was detected and repaired during the inspection of the tank in 1990 [26]. The crack growth analysis predicts a critical crack depth of 1.17 inches, approximately ¼ of the wall thickness, where the stress intensity factor in the depth direction exceeds K_{Ie}. K_{Ie}, as opposed to K_{IC}, is the controlling factor in this case because the critical crack is a part-through crack [30]. The cycles to failure are 44,721, where one cycle equates to one pressurization cycle of the LOX tank. Figure 25 depicts the crack size relative to the geometry and Figure 26 shows the remaining cycles to failure for any given crack size from this analysis. Running the same analysis with an initial crack size of 0.1 inches resulted in 131,923 cycles to failure.

All subsequent sensitivity studies are performed using the initial crack size of 0.5 inches. The fracture toughness was varied from the baseline (83 ksi $in^{1/2}$) to simulate a very low toughness weld (K_{IC} = 40 ksi $in^{1/2}$). The apparent fracture toughness was held to be 1.4 times the plane strain fracture toughness based on the relationship between the two values for the base material, *i.e.* K_{Ie} = 1.4 K_{IC}. This relationship between K_{Ie} and K_{IC} is common for austenitic stainless steels based on data found in the NASGRO material database [1]. Variation of the fracture toughness and the resultant cycles to failure and critical crack size is plotted in Figure 27. The variation is similar to an S-shaped curve with a large linear portion. If the toughness drops to 60 ksi $in^{1/2}$ then the predicted cycles to failure will be approximately 23,748 cycles, whereas a drop in toughness to 50 ksi $in^{1/2}$ yields a failure time of 9,764 cycles compared to the baseline of 44,721 cycles.

Finally, the residual stresses due to the repair are modified based on observations from the nuclear industry to be the flow stress (62.5 ksi) locally and linearly decay to zero at ¾ of the thickness in both the thickness and width directions. The result of changing the repair residual stress from 35 ksi to 62.5 ksi decreases the cycles to failure from 44,721 to 20,647.

Summary

The damage tolerance analysis of the LOX tank focused on crack growth between Nozzles V and N because of the following assumptions:

1. Nozzle V experiences the greatest thermal stresses during tank pressurization.
2. Nozzle N experiences the greatest pressure stresses during tank pressurization.
3. A crack was found at Nozzle V during the dye penetrant inspection and weld repaired.
4. The weld repair at Nozzle V induced a residual stress that would assist crack propagation.

The geometry of the LOX tank section between Nozzles V and N was modeled using a thick plate 4.73 inches thick by 7 inches wide to encompass both the distance between the Nozzles and the weldments on each side connecting the Nozzles to the tank. Conservatisms built into the geometry assumption are:

1. The geometric model does not account for any stiffness of the surrounding tank or Nozzles.

The stress distribution applied to the crack growth model was nonlinear in both the thickness and width directions to accurately describe the stress distributions of the tank pressure, thermal stress and residual stresses from both construction and repair welding. Conservatisms built into the stress profiles are:

1. The thermal stresses have a factor of ten applied to the heat transfer coefficient, increasing the thermal stress magnitude above what would be expected.
2. The thermal stress is assumed constant between the Nozzles, when it decays rapidly from Nozzle V.
3. The residual stresses from construction are considered to be 15% of the room temperature yield stress (due to post-construction stress-relief), when the literature suggests the residual stresses should be closer to zero.
4. The residual stresses from the repair weld are tensile through the entire weld nugget and heat-affected zone and then drop to zero stress instead of a beneficial compressive stress.

The mechanical material properties were taken from data generated during the construction and repair of the tank. The crack growth rate data was taken from the NASGRO material database to fit the high stress ratio data of 304 stainless steel at cryogenic temperature. Conservatisms in the material properties are:

1. The crack growth rate curve is nearly a factor of two more conservative than the NASGRO standard curve and is an upper bound for all data.

The initial crack size is assumed to be 0.5 inches, which corresponds to a crack that was detected and repaired in 1990. The NASA standard for damage tolerance inspection, NASA STD-5009 recommends an initial crack size of 0.1 inches in radius based on inspection method, in this case fluorescent penetrant, and geometry. Conservatisms in the initial crack size are:

1. The initial crack size of 0.5 inches used in the analysis is five times that recommended by NASA STD-5009.

A summary of the all the crack growth analyses performed based on different assumptions is presented in Table 6.

The damage tolerance analysis performed using NASGRO 4.22 predicts that a one-half inch corner crack would fracture the ligament between Nozzle V towards Nozzle N in 44,721 pressurization cycles. The NASA STD-5003 requires pressure vessels that have a catastrophic failure mode, such as the LOX tank, have an inspection interval of one-fourth the total damage tolerance lifetime. Therefore, the NASA standards would recommend a maximum time between inspections of 10,000 cycles.

Taking into account the current state of the tank, reducing the recommended inspection interval to 1,000 pressurization cycles would increase the factor of safety on the damage tolerance analysis to forty. To understand what a recommended 1,000 cycle inspection program would provide as a factor of safety, parametric studies were performed to evaluate the sensitivity of the damage tolerance analysis to the material fracture toughness because of uncertainties in the welding process. Presuming the factor of four on lifetimes (*i.e.* the total life is 4,000 cycles), the fracture toughness of the weld could be as low as approximately fifty percent (~ 45 ksi $in^{1/2}$) of the reported value. Including the conservatisms built into the base analysis predicting 44,721 cycles to failure, an inspection interval of 1,000 cycles is very conservative.

Acknowledgements

The authors would like to thank J. Brady, E. Glaessgen, I. Raju, J. Newman, and the NASA Langley Pressure Systems Committee for their valuable insight and guidance in these analyses.

Reference

[1] NASGRO Version 4.22, nasgro.swri.org, managed by Southwest Research Institute, San Antonio, TX.
[2]*Material & Welder's Record*, Southwest Welding & MFG. Co., Rocketdyne Contract R-943-C-F-972, 1959
[3] *ASME-BPVC*, Section VIII, Division 1, Rules for Construction of Pressure Vessels – Division 1, 2004.
[4] *ASME-BPVC*, Section IX, Qualification Standard for Welding and Brazing Procedures, Welders, Brazers, and Welding and Brazing Operators, 2004.
[5] *Source Book on Stainless Steels*, Metals Engineering Institute, ASM International, Metals Park, OH, 1979.
[6] *Metals Handbook Tenth Ed.*, Volume 1: Properties and Selection: Irons, Steels, and High-Performance Alloys, ASM International, Metals Park, OH, 1990, pp. 841-907.
[7] *ASME BPVC*, Section II, Part A, Materials - Ferrous Material Specifications, 2004.
[8] Thomas, Jr., R.D. and Messler, Jr., R. W. "Welding Type 347 Stainless Steel-An Interpretive Report," *Welding Research Council Bulletin 421*, May 1997.
[9] Stainless Steels Types 321, 347 and 348, *Allegheny Technologies Inc*., Allegheny Ludlum Technical Data Blue Sheet, 2003.
[10] Drawing No. D-9093: Nozzle N Blended Weld & Forging Proposals, Southwest Welding & Mfg. Co., dated 3-25-1959.
[11] ANSI/AWS A5.4-92, Specification for Stainless Steel Electrodes for Shielded Metal Arc Welding, American Welding Society, 1992.

[12] Welding Handbook Ninth Ed., Volume 2: Welding Procecesss, Part 1, American Welding Society, Miami, FL, 2004.
[13] Welding Handbook Eighth Ed., Volume 4: Materials and Applications – Part 2, American Welding Society, Miami, FL, 1998.
[14] Welding Handbook Ninth Ed., Volume 1: Welding Science & Technology, American Welding Society, Miami, FL, 2004.
[15] ASME-BPVC, Section II, Part C, Materials-Specifications for Welding Rods, Electrodes, 2004.
[16] Welding Procedure Specification No. G-4274 # 1, dated 1-17-65.
[17] Military Specification MIL-E-22200 / 2D Electrodes, Welding, Covered (Austenitic Chromium-Nickel Steel), September 1986.
[18] ANSI/AWS A5.9-93, Specification for Bare Stainless Steel Welding Electrodes and Rods, American Welding Society, 1993.
[19] Pro/ENGINEER Version 2.0, www.ptc.com, The Product Development Company, 2005.
[20] Pro/MECHANICA, www.ptc.com, The Product Development Company, 2005.
[21] Patran, www.mscsoftware.com, MSC Software, 2005.
[22] Abaqus, www.abaqus.com, Dassault Systémes, 2005.
[23] Nastran, www.mscsoftware.com, MSC Software, 2005
[24] Kays, W. M. and Crawford, M.E, *Convective Heat and Mass Transfe*r; McGraw-Hill: New York, USA, 1980.
[25] Residual Stress Effects in Fatigue, ASTM STP 776, ASTM, 1981.
[26] Report of Welded Repair for LOX Run Tank, NASA Contract No. 18367C, 1991.
[27] *Nondestructive Evaluation Requirements for Fracture Control Programs*, NASA STD 5009, 2003.
[28] *Damage Tolerant Design Handbook*, Volume 1, December 1983.
[29] J. M. Barsom and S. T. Rolfe, *Fracture & Fatigue Control in Structures, Applications of Fracture Mechanics*, 2nd ed., Prentice-Hall, Inc., 1987, pp. 159-188.
[30] Forman, R.G., and Henkener, J.A., "An Evaluation of the Fatigue Crack Growth and Fracture Toughness Properties of Beryllium-Copper Alloy CDA172," *NASA Technical Memorandum 102166*, 1990.

Figure 1. Schematic of the Liquid Oxygen (LOX) tank construction. Black lines indicate welds.

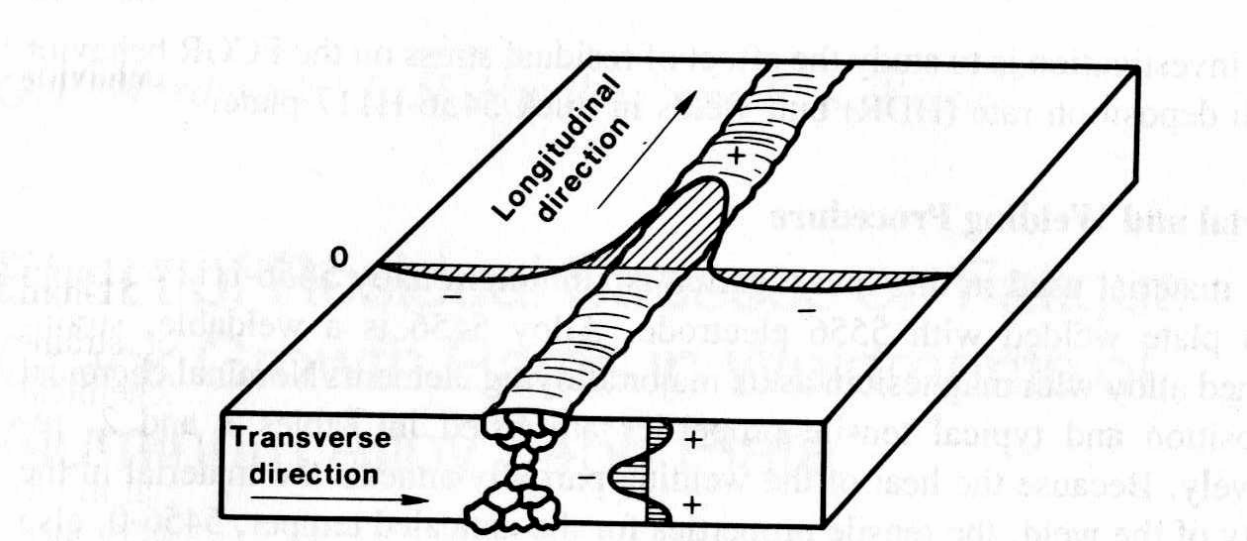

Figure 2. Drawing showing residual stress orientation in a conventional welded plate. [7, 8].

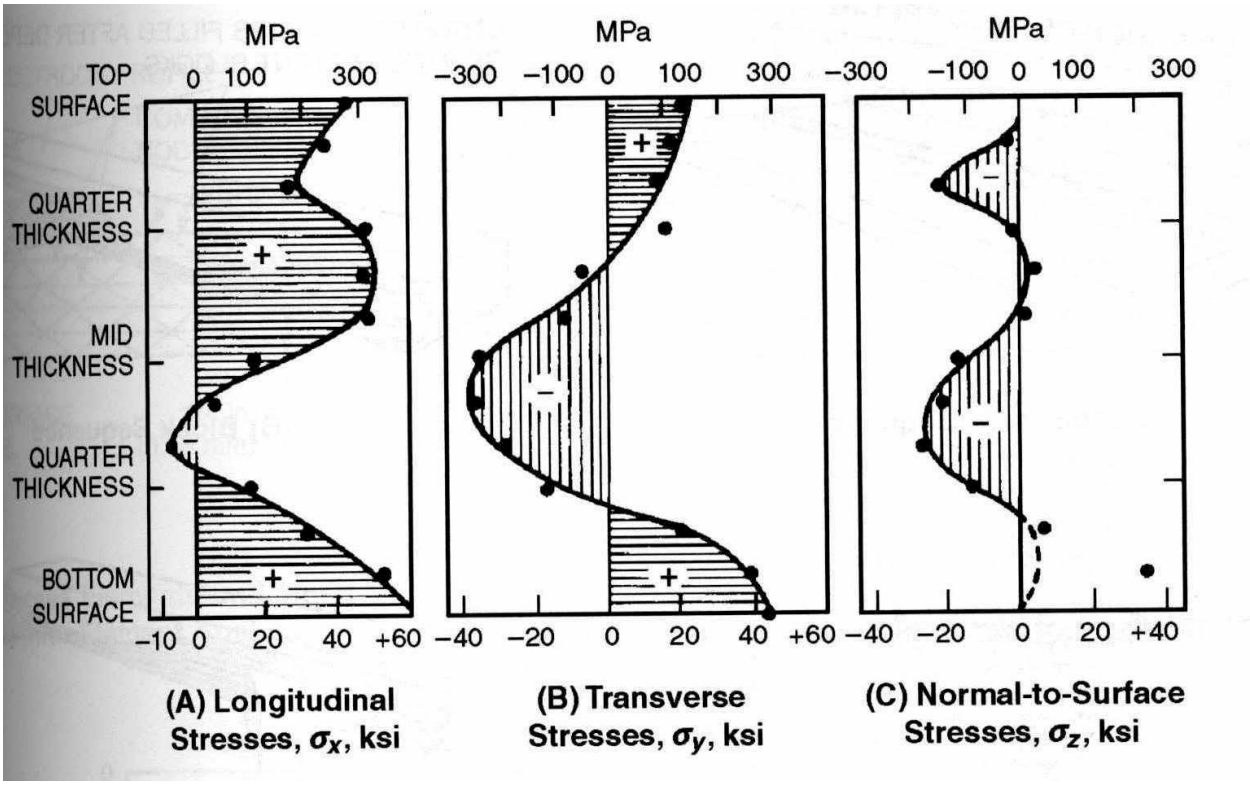

Figure 3. Schematic showing residual stress distribution in a conventional welded plate (indicated directions are with respect to the weld) and level of residual stresses. [7, 8].

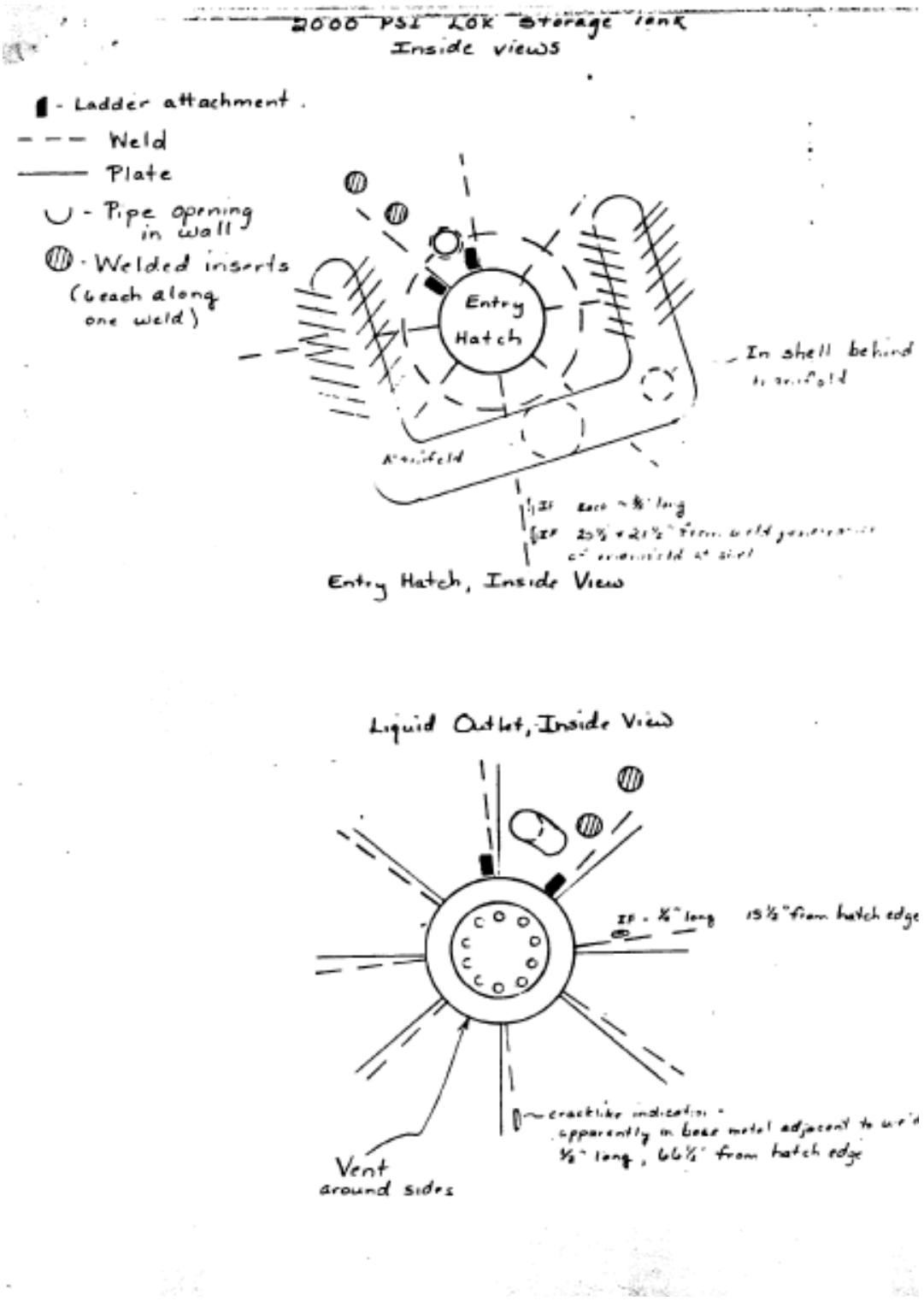

Figure 4. Schematic showing weld modifications of the plugs to the LOX tank [26].

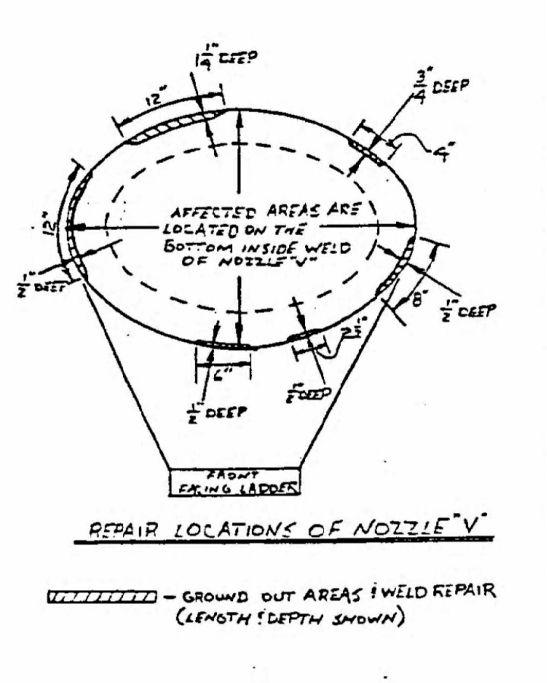

Figure 5. Repair drawing for Nozzle V of the LOX tank [26].

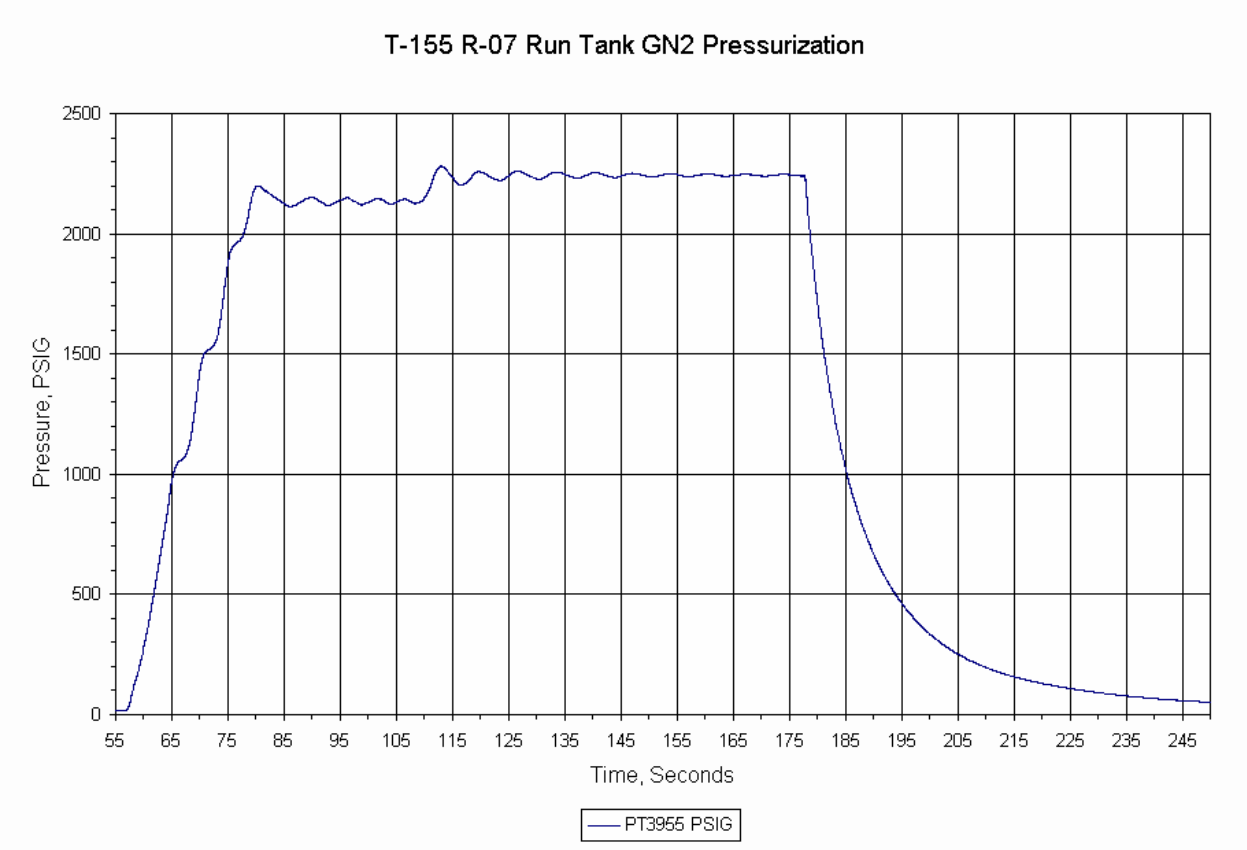

Figure 6. Pressurization profile of the LOX tank.

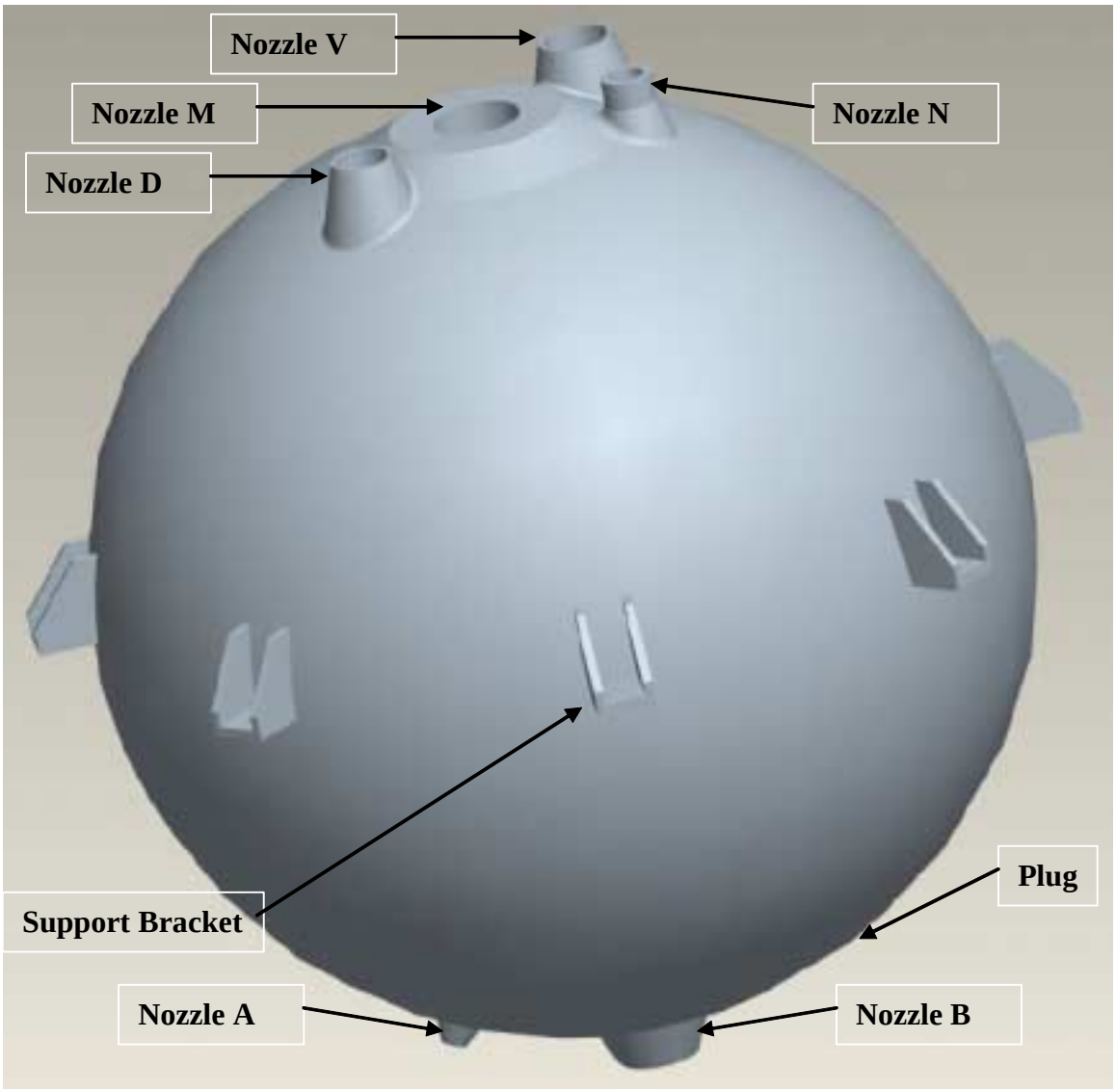

Figure 7. Pro-Engineer model of the LOX tank.

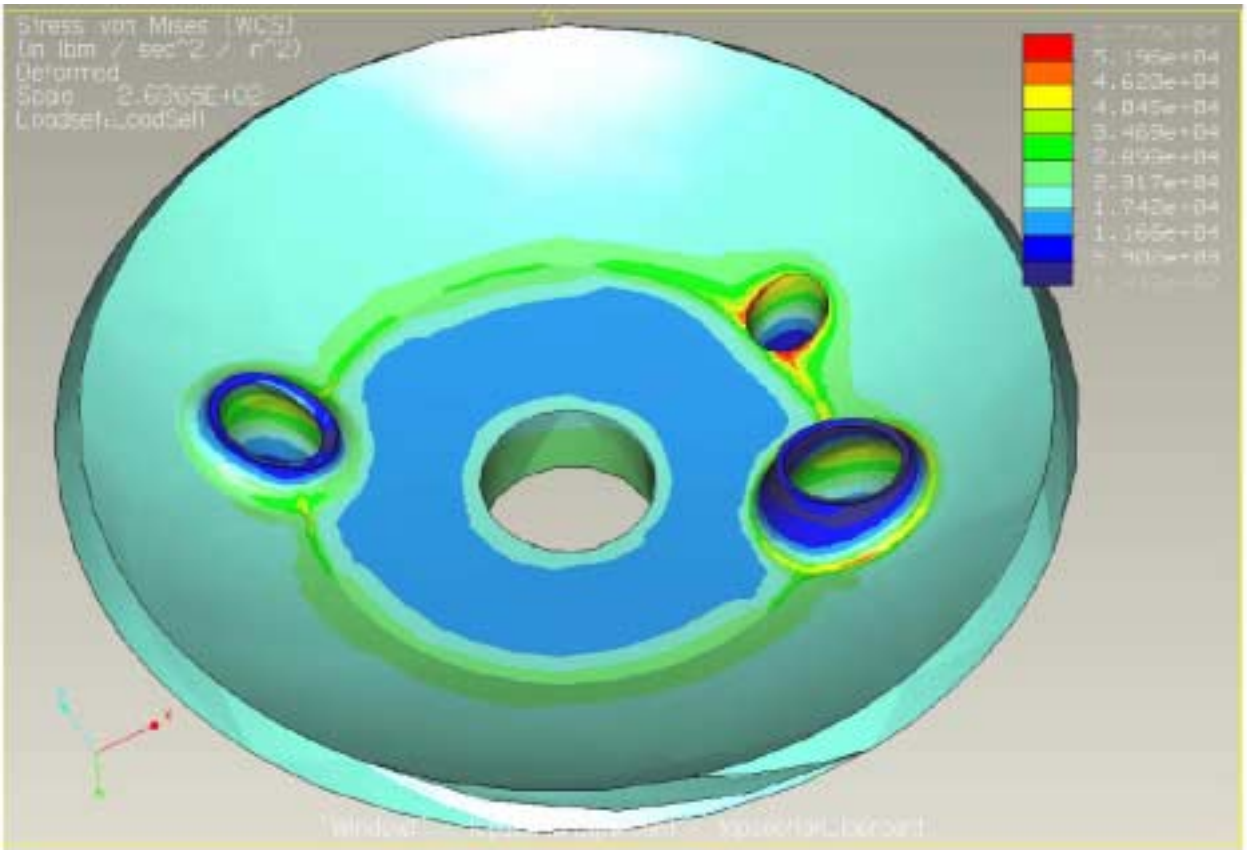

Figure 8. Von-Mises stresses for the inside of the top of the LOX tank modeled using Mechanica.

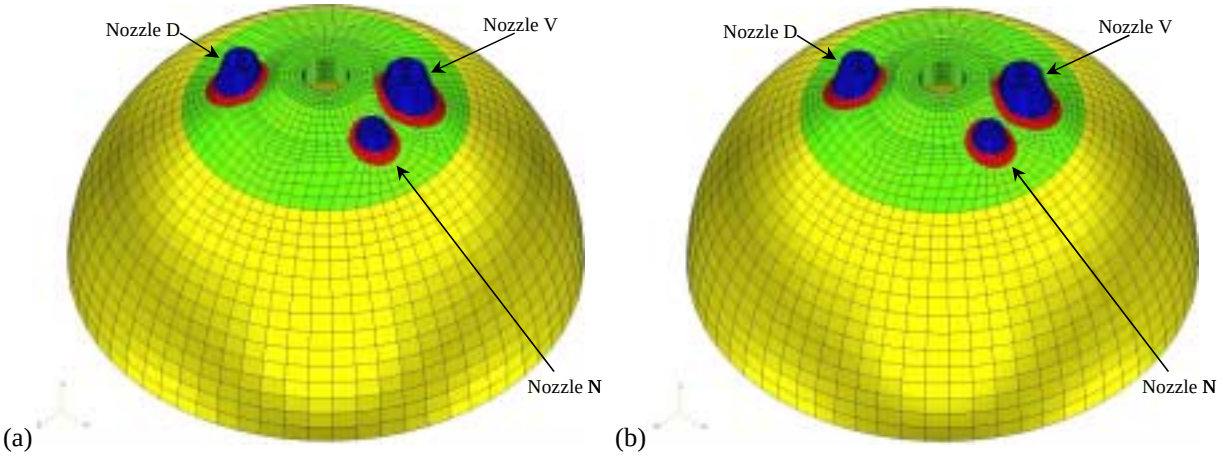

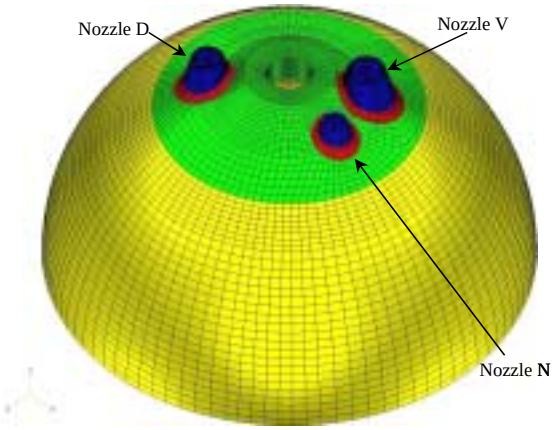

(c)

Figure 9. Patran models with (a) course, (b) medium, and (c) fine mesh refinement of the upper portion of the LOX tank.

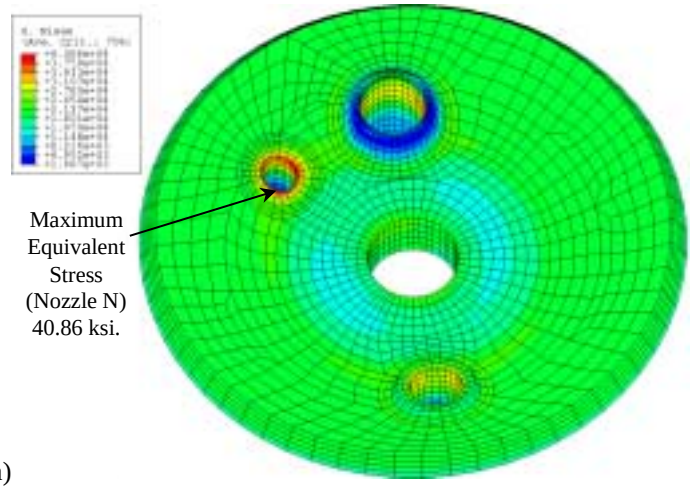

(a)

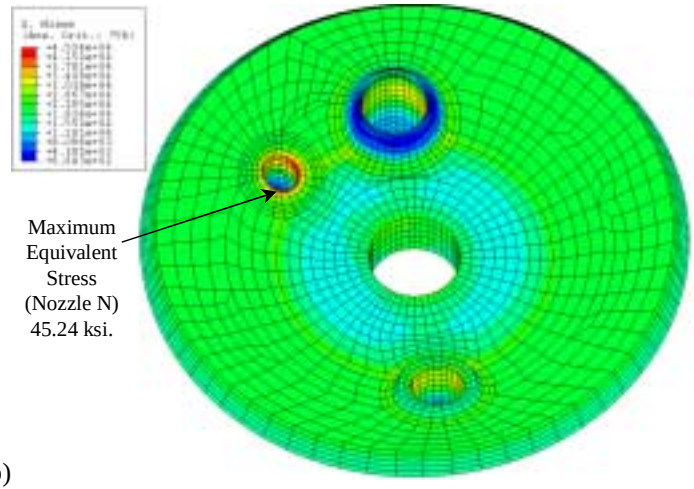

(b)

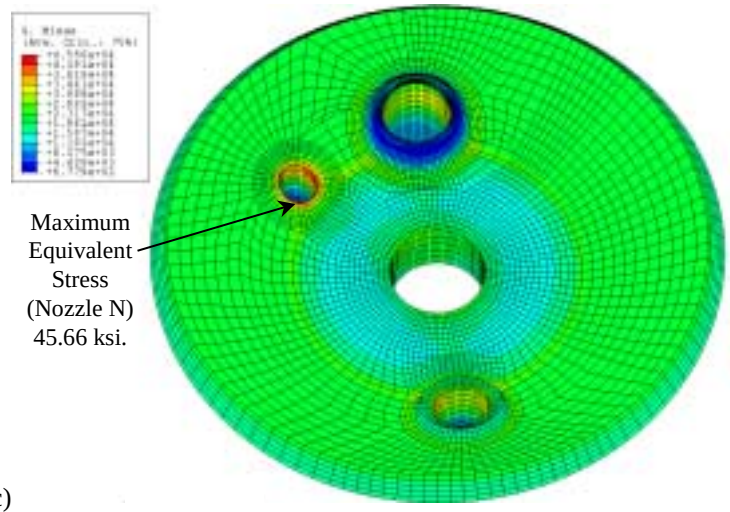

(c)

Figure 10. Von-Mises stress plots from Abaqus with (a) course, (b) medium, and (c) fine mesh refinement of the upper portion of the LOX tank.

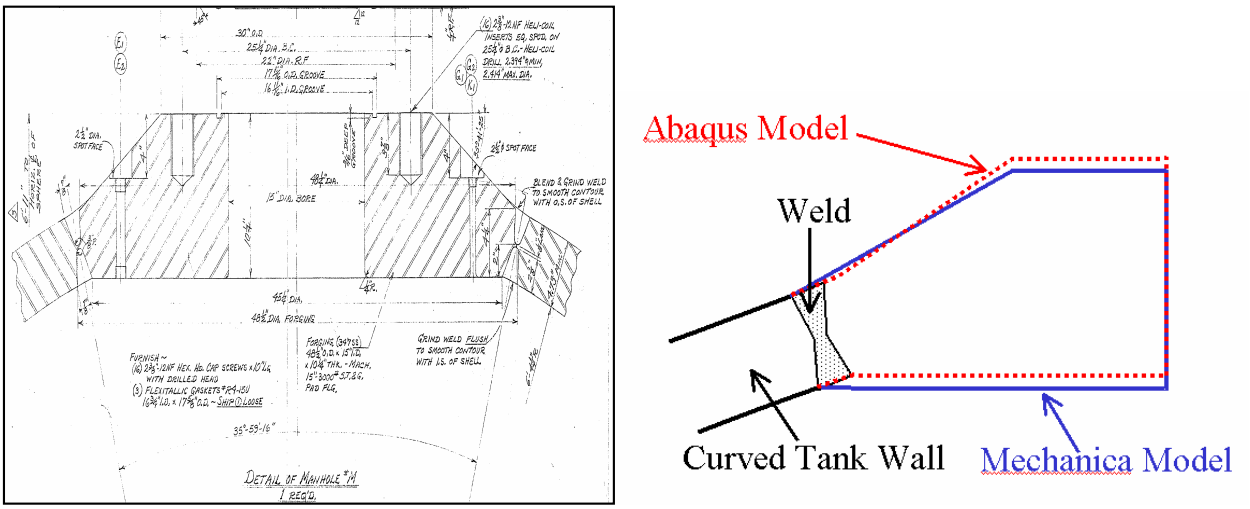

Figure 11. Comparison of Mechanica and Abaqus mesh details.

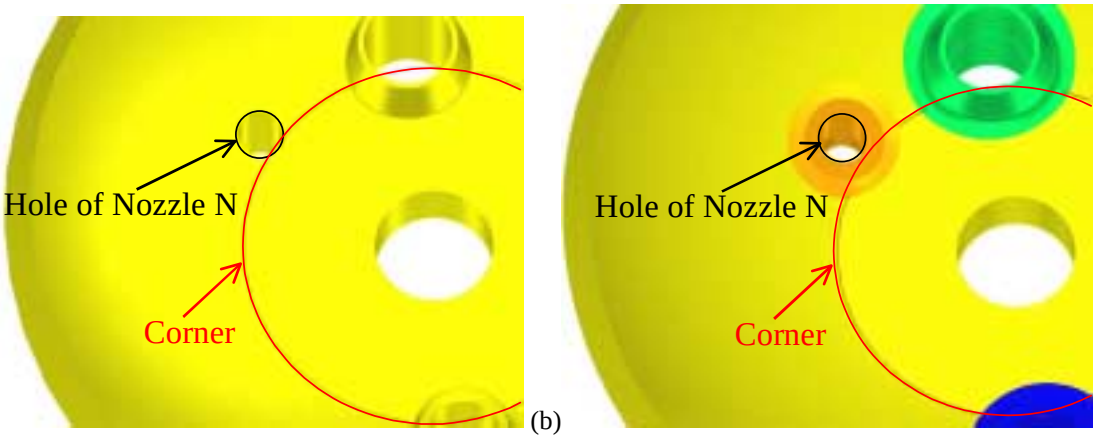

(a) (b)

Figure 12. Comparison of (a) Mechanica and (b) Abaqus geomtry details at Nozzle N.

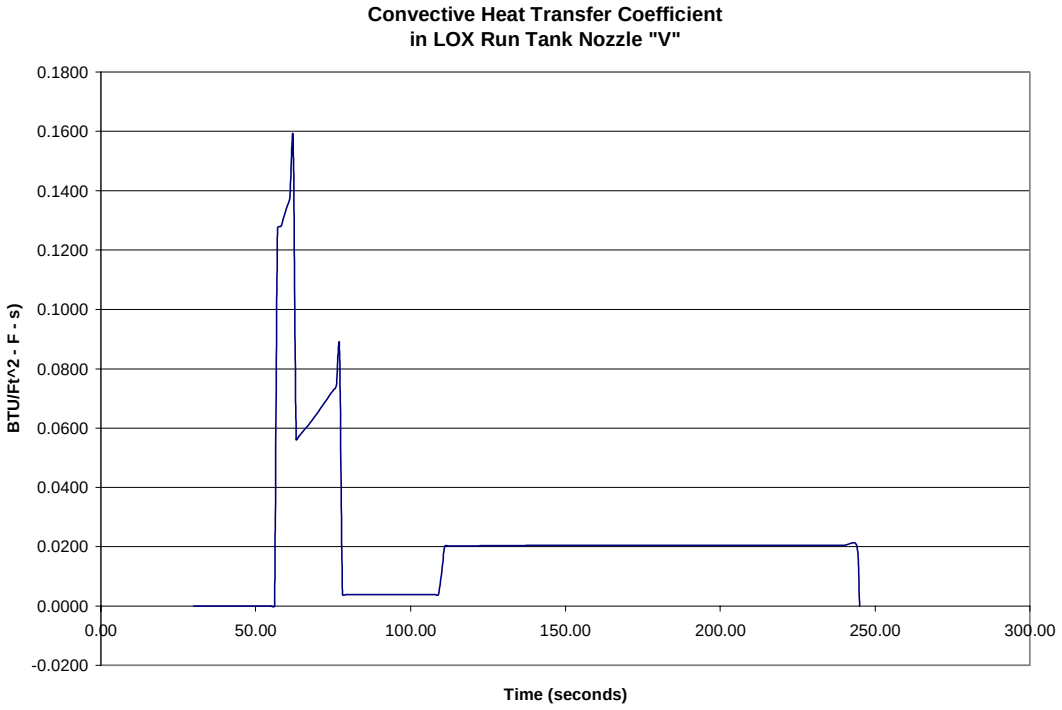

Figure 13. Heat transfer coefficient versus time during LOX tank operation at Nozzle V.

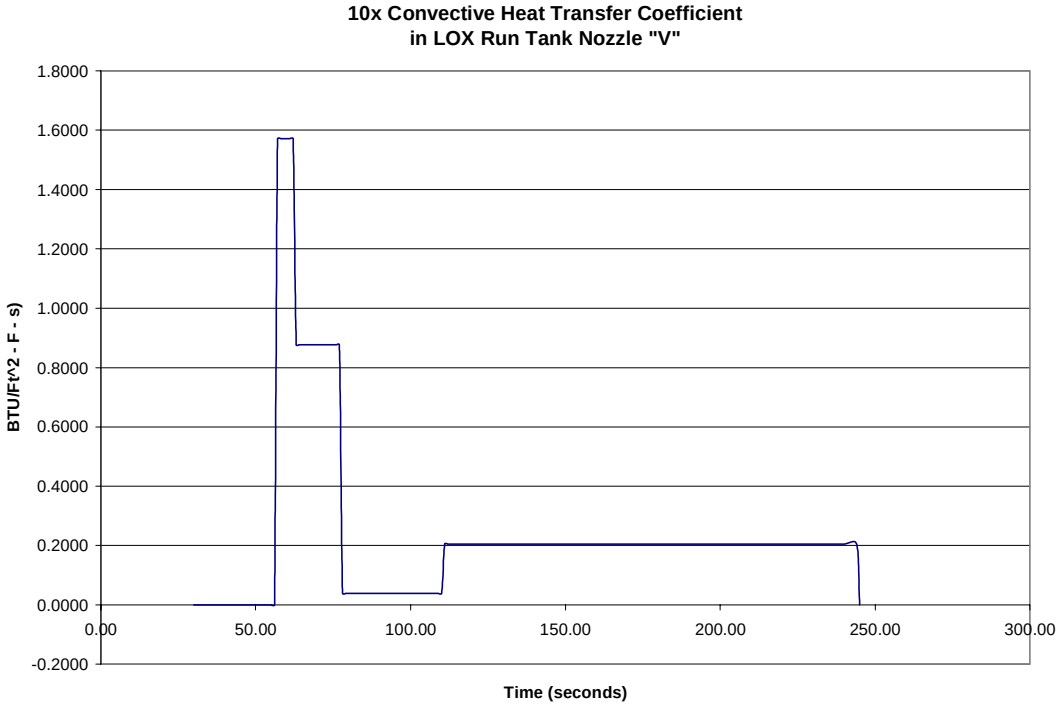

Figure 14. Conservative estimate of the heat transfer coefficient versus time at Nozzle V used for the Nastran analyses.

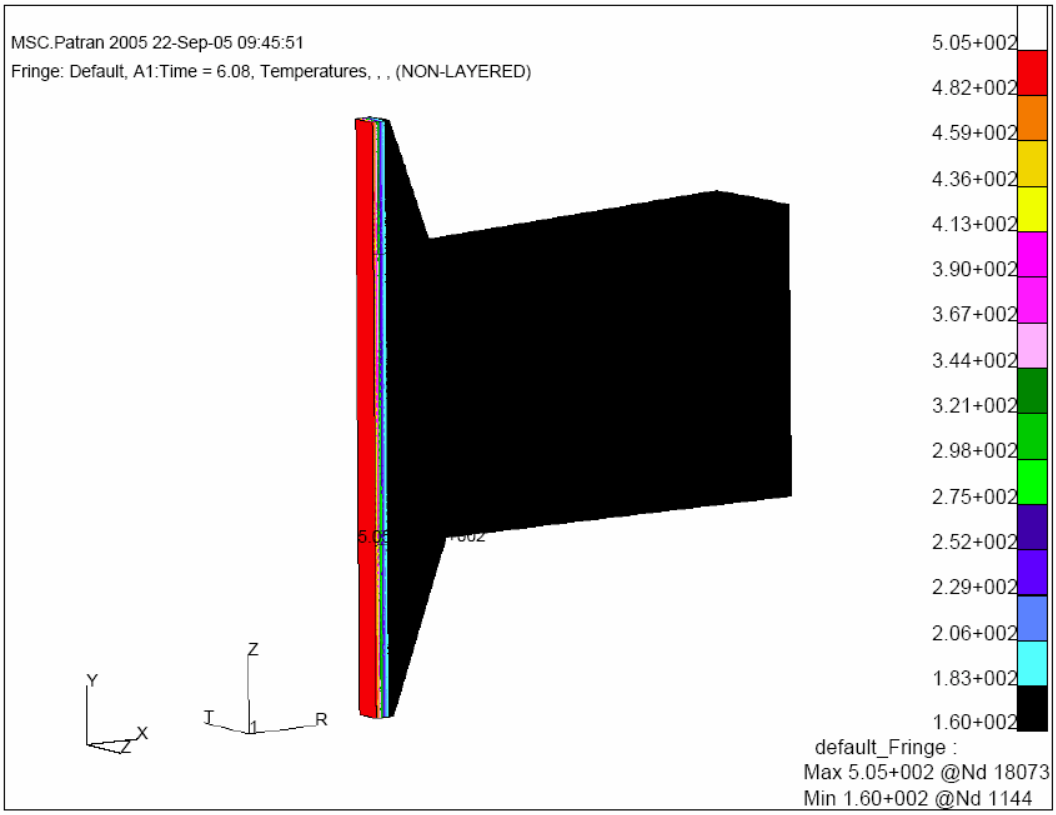

Figure 15. Nozzle V temperature gradient, Ro, at 62 seconds.

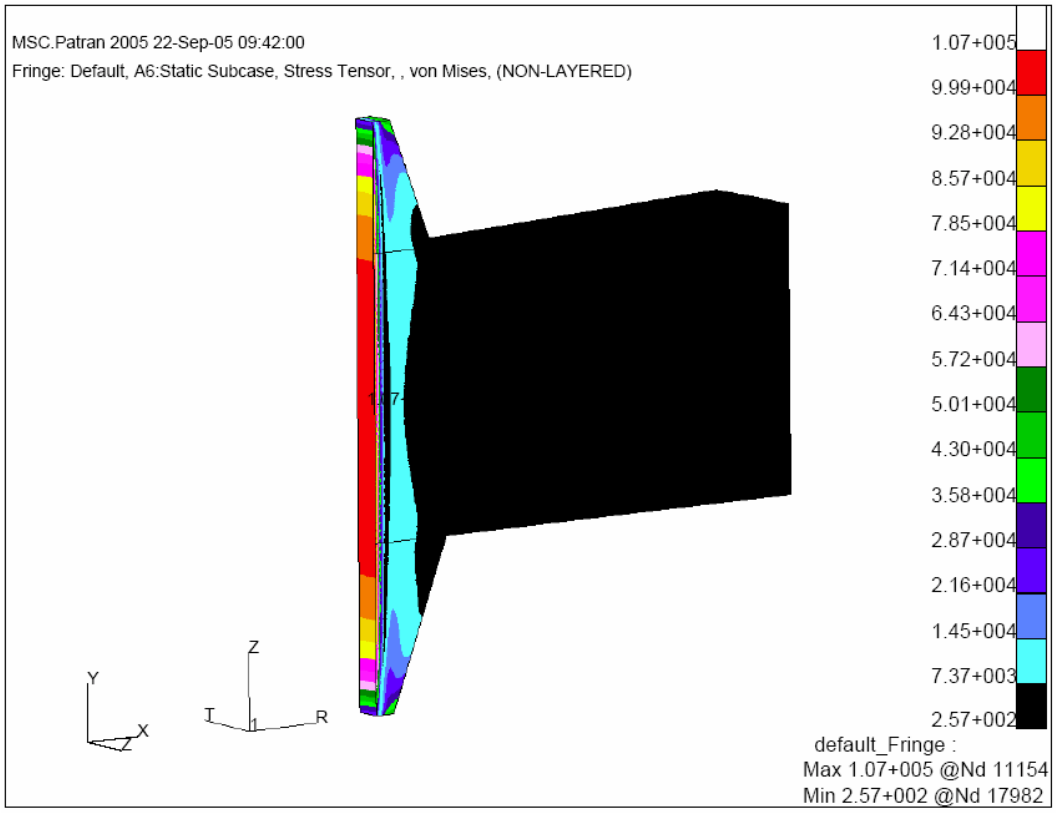

Figure 16. Nozzle V von Mises thermal stress gradient at 62 seconds.

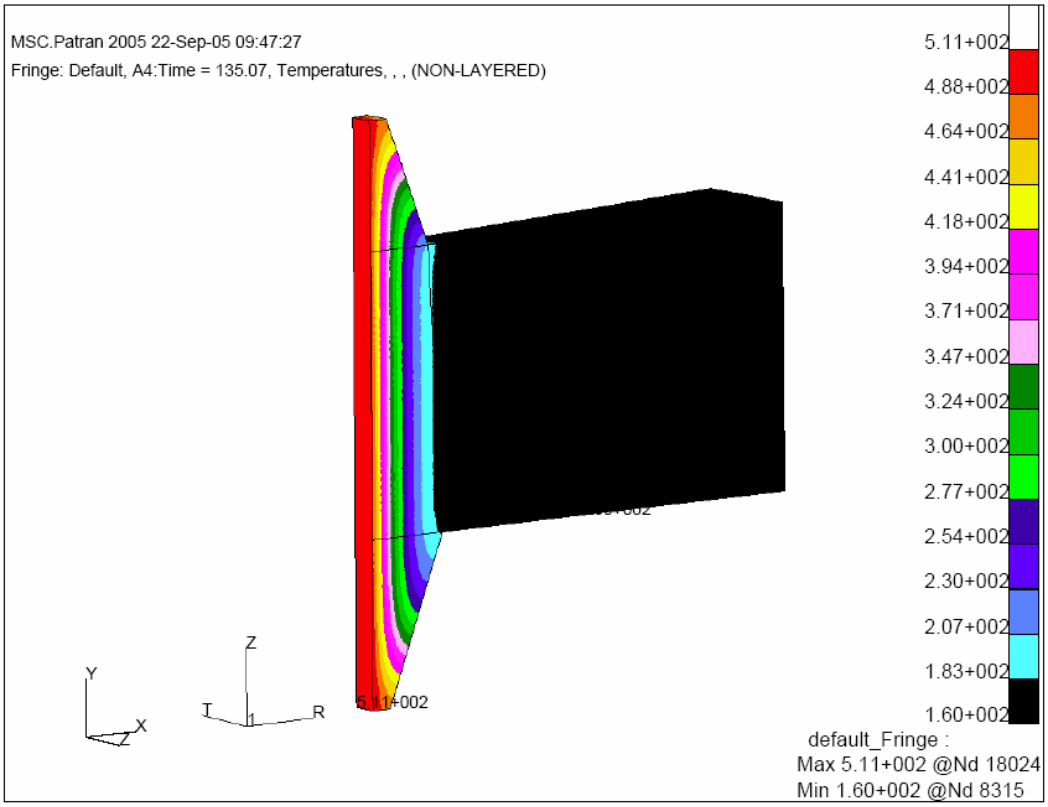

Figure 17. Nozzle V temperature gradient, Ro, at 245 seconds.

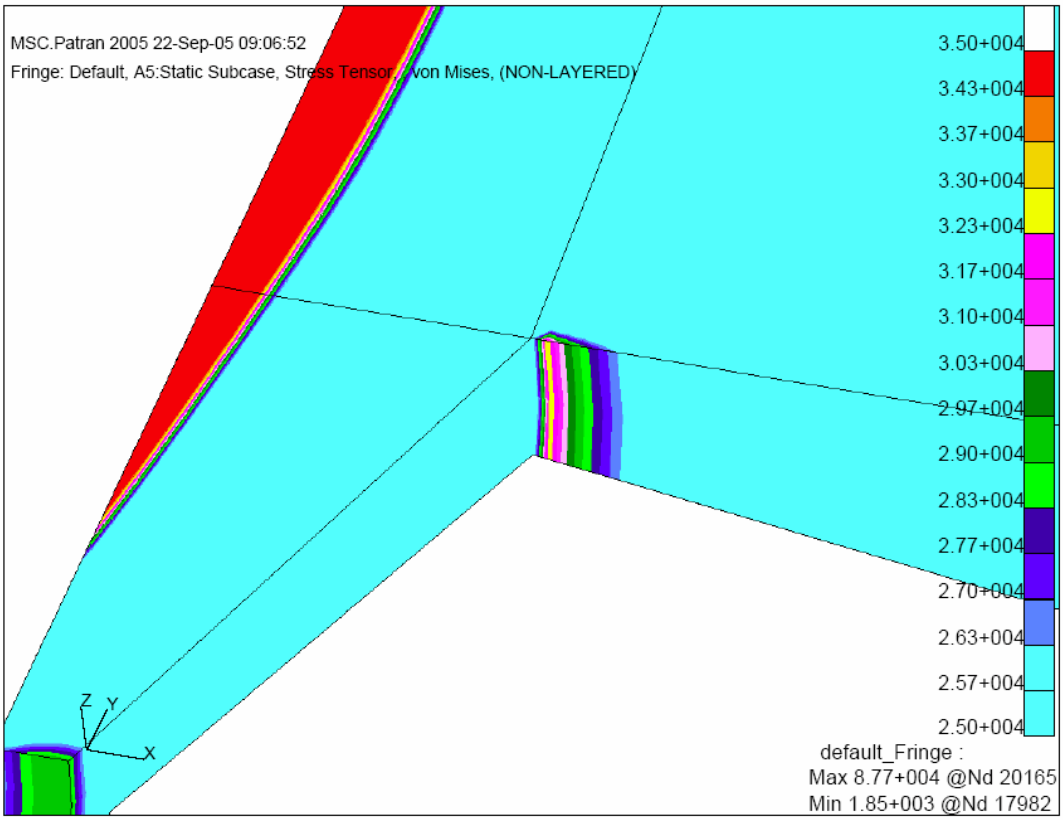

Figure 18. Nozzle V von Mises thermal stress gradient at 245 seconds.

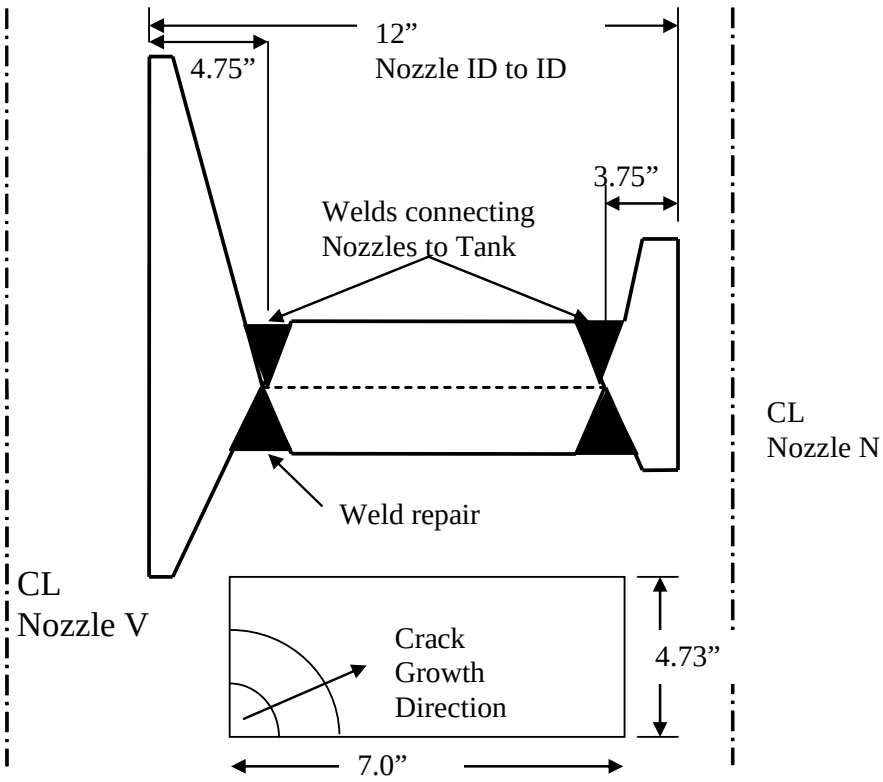

Figure 19. Diagram of the geometry assumed for the crack growth model (Not to Scale).

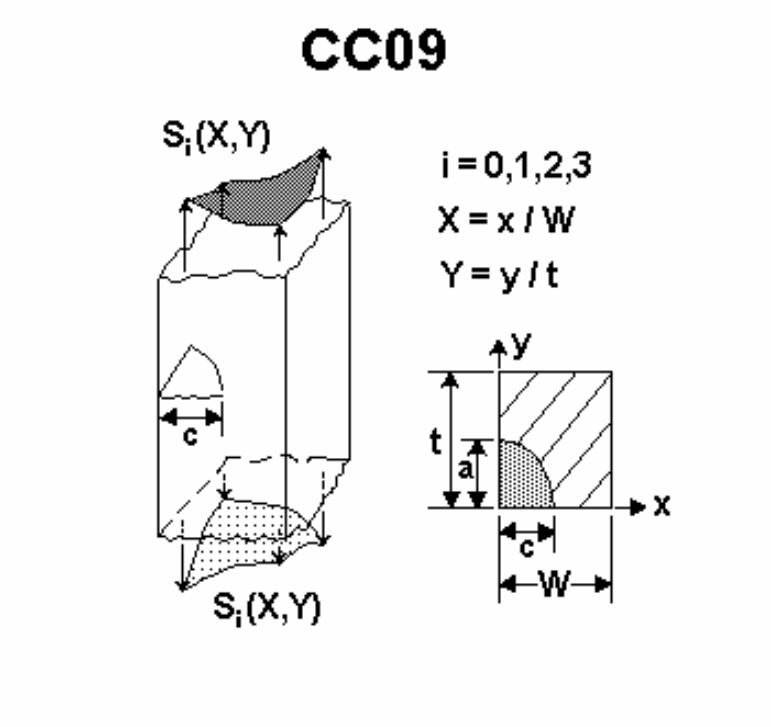

Figure 20. Corner crack in a thick plate model used to simulate cracking in a nonlinear stress field from Nozzle V to Nozzle N.

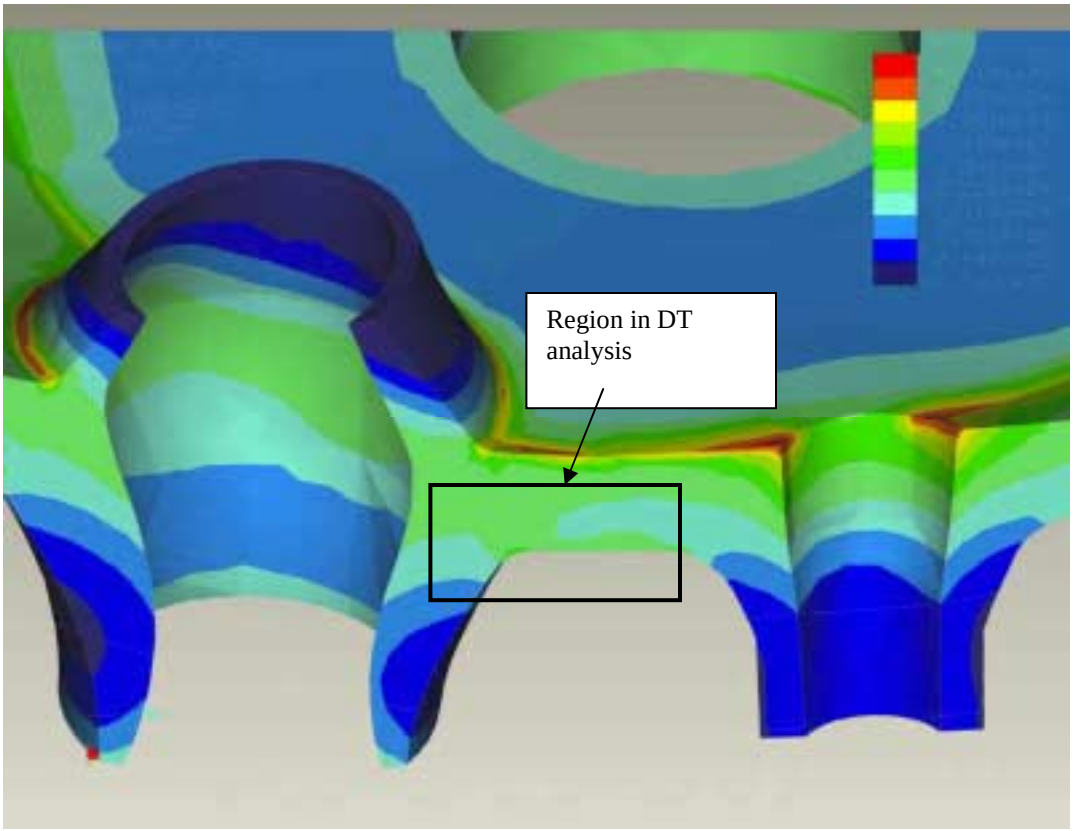

Figure 21. Principal pressure stress used for the damage tolerance analysis.

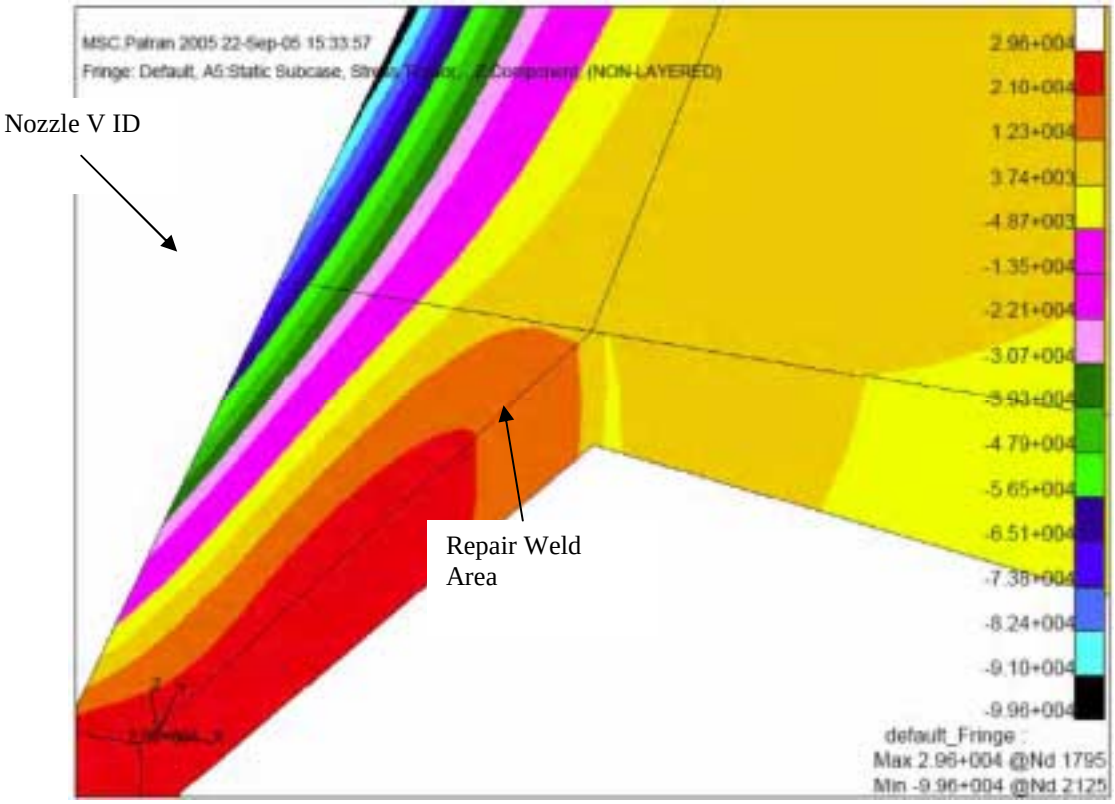

Figure 22. Thermal stress cycle of Nozzle V in the hoop direction (z) at 245 seconds.

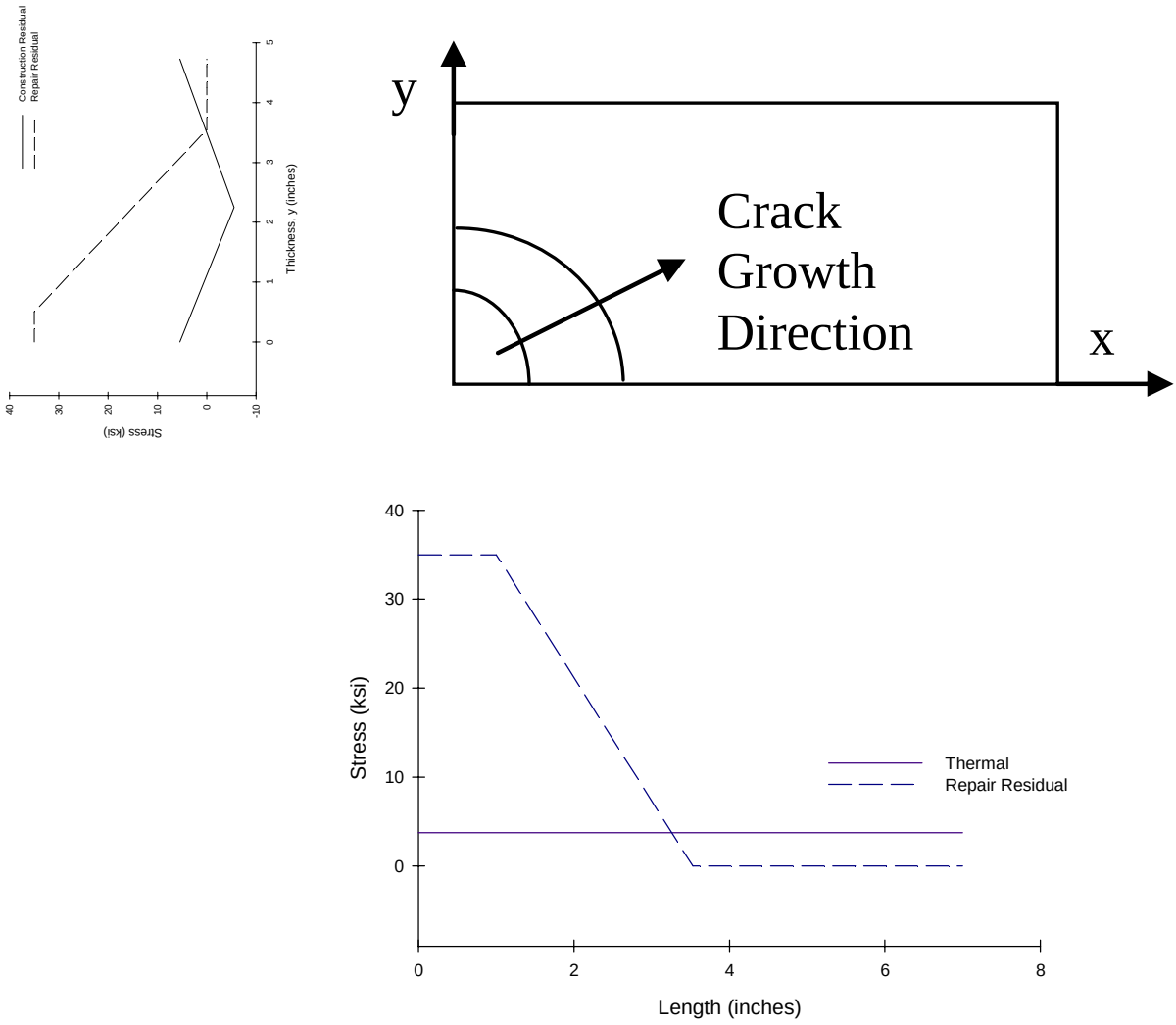

Figure 23. Residual stress profiles in the vicinity of Nozzle V.

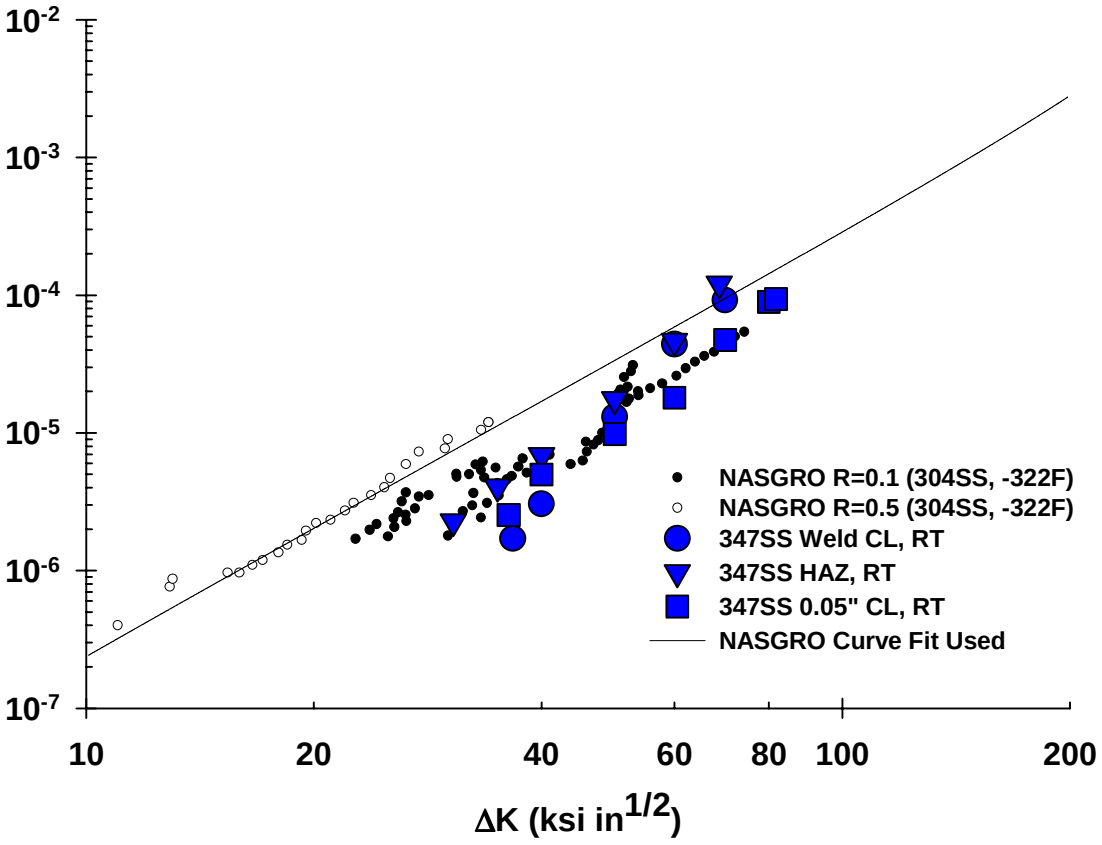

Figure 24. Fatigue crack growth rate data and curve-fit used for the NASGRO damage tolerance analyses.

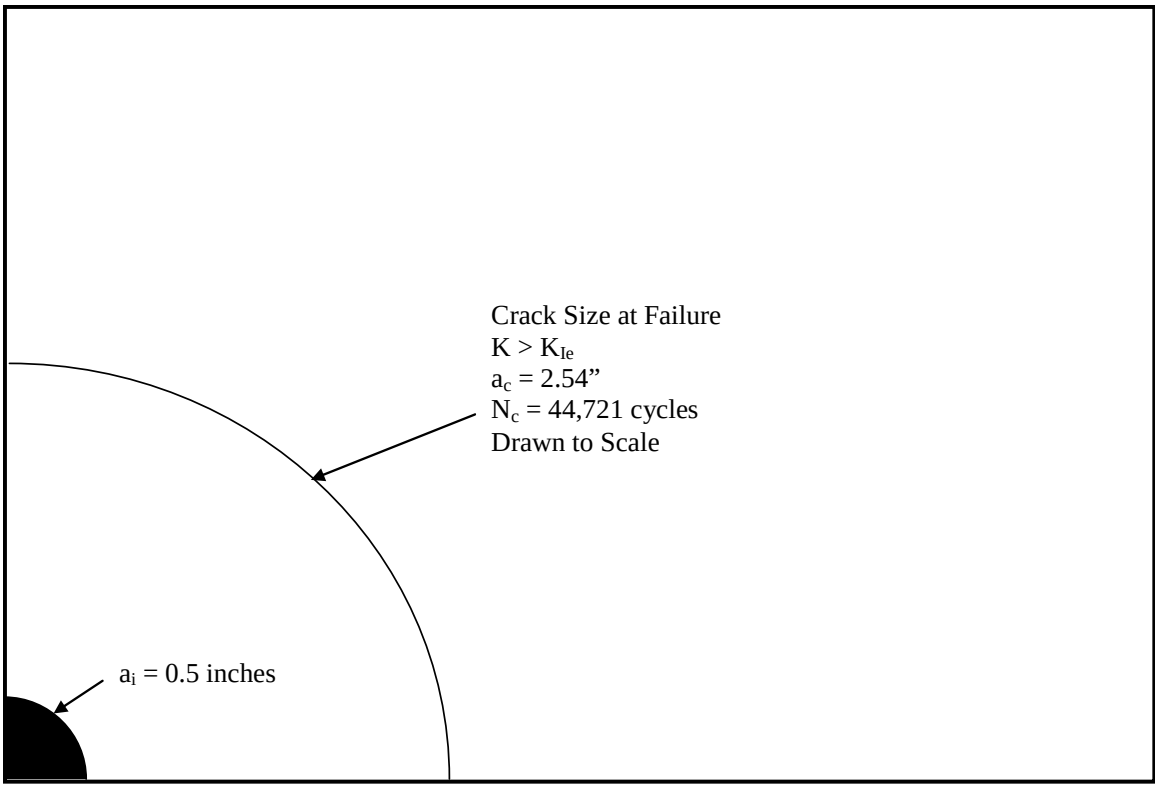

Figure 25. Graphical representation of the damage tolerance analysis for a ½ inch crack to failure.

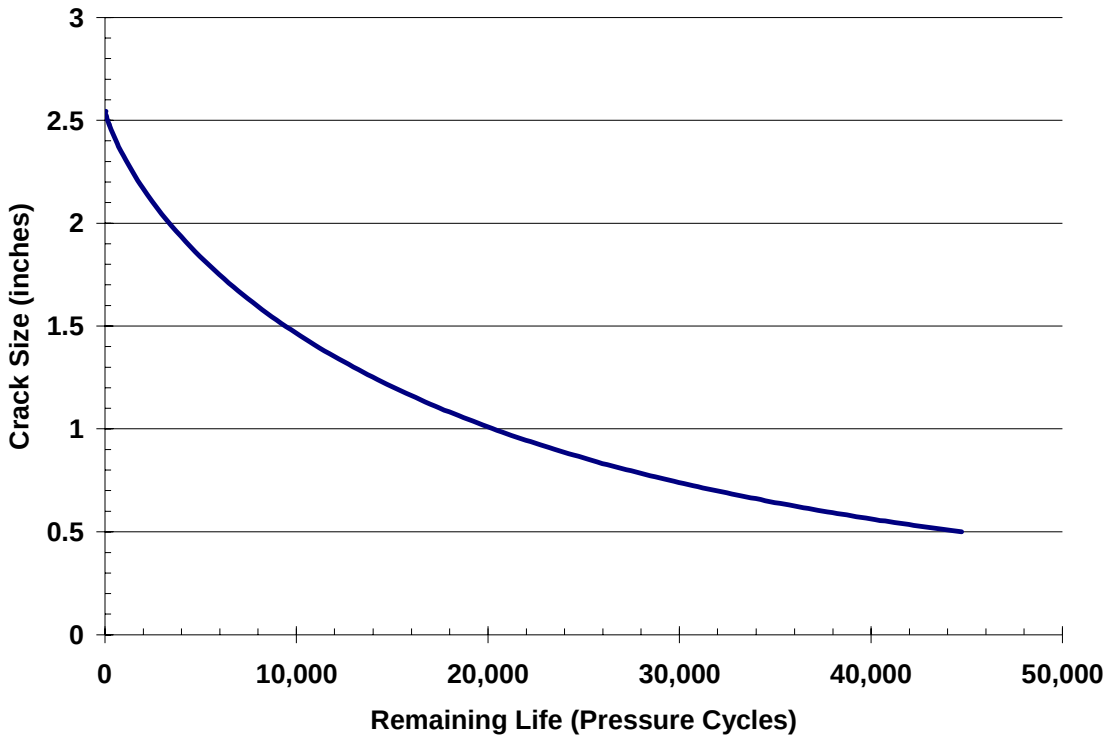

Figure 26. Crack size versus remaining life generated from the damage tolerance analysis of a ½ inch crack to failure.

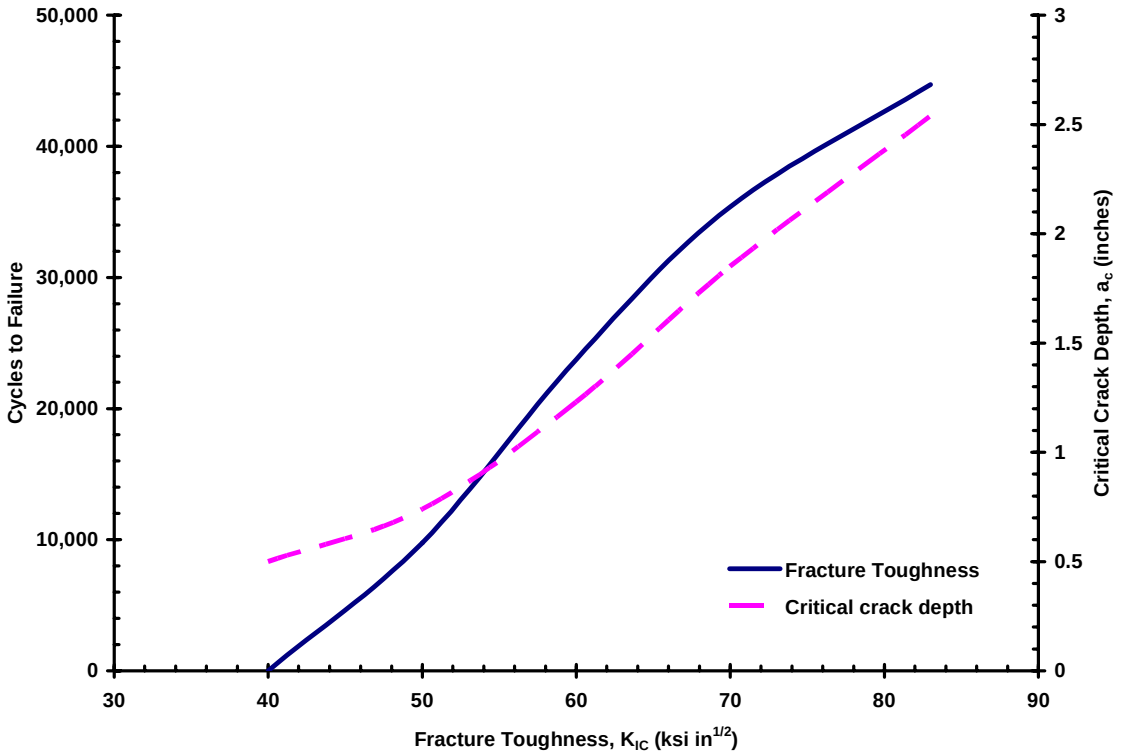

Figure 27. Cycles to failure and critical crack depth versus fracture toughness generated from the damage tolerance analysis of a ½ inch crack to failure.

Table 1. Typical tensile properties of annealed 347 stainless steels [5]

Product Form	Temp °F	UTS, ksi	YS, ksi	Elong, %	Reduct. Area, %	E, Msi	Charpy-V, ft-lb
347 sheet, plate	75	94	37	52	----		120
	-320	198	61	47	----		66
347 bar	75	97.4	49.3	57	76	28.3	
	-320	214	62.2	43	60	30.3	

Table 2. Qualifying Mechanical Properties of 347 Weld Metal at -320°F

WELD METAL TEST RESULTS - rec'd via telecon from W. Vetter on 31 March 1959
Project 00218

			UTS psi	YS psi	Elongation (in 2 in.) %	Reduction Area %
Weld Metal	Sample 3	Ambient	81,090	48,450	42.9	40.3
	Sample 4	Ambient	81,040	47,220	32.0	31.1
	Sample 1	-320°F	173,470	48,890	36.6	29.9
	Sample 2	-320°F	132,620	50,000	19.9	17.1

Table 3. Qualifying Mechanical Properties of 347 Base Material and Weld Metal at -320°F

MATERIAL REORTS FOR 8000 GALLON LOX SPHERE
test results for low temperature tensile and Charpy Impact

Component	Heat No.	Slab No.	UTS psi	YS psi	Elongation (in 2 in.) %	Reduction Area %	Charpy Impact ft-lbs
Weld metal			173,700	---	25.0	25.3	18.5, 18.5, 16.75
			169,500	---	32.0	30.1	
(retest of above)			173,476	48,894	36.6	29.9	not required
Plate:	336438	1	166,200	75,900	26.0	55.5	57, 56, 57
4-5/8" segments	336438	2	156,900	68,800	25.0	58.7	48, 49, 50
	336439	1	170,000	72,700	27.0	56.4	49, 46, 48
	336439	2	196,300	73,400	28.0	53.2	50, 49, 54
	336440	1	190,800	70,600	28.0	53.2	51, 49, 56
	336440	2	210,300	79,400	32.0	50.5	45, 44, 43
	336441	1	154,500	72,700	30.0	58.2	41, 45, 45
	336441	2	204,600	87,200	33.0	51.4	36, 35, 35
Flanges	40242		194,187	44,914	55.4	59.1	77, 75, 73
(forgings for	78501		225,500	---	32.3	39.7	57, 55, 48
manhole & nozzles)	78505		210,200	---	33.5	36.9	58, 40, 49
(Retest)	78501		205,641	48,225	45.7	51.0	not required
(Retest)	78505		213,845	40,427	44.0	51.5	not required
	78579		193,840	37,681	36.0	26.3	45, 36, 49
	4007		207,911	34,956	42.9	48.5	39, 41, 44
			205,641	43,676	45.7	42.8	39, 41, 44
(Retest)	4007		207,461	46,769	43.6	47.9	not required

Table 4. Chemical Analysis of the 347 Stainless Steel LOX Run Tank Sphere Segments

Chemistry Analysis for Sphere Segments of LOX Vessel (Inner Sphere), wt %

Manufacturer	ASTM Spec.	Heat No.	C	Mn	P	S	Si	Cr	Ni	Cb	Ta	Cb+Ta
Allegheny	347	336438	0.044	1.69	0.024	0.011	0.55	17.65	9.46	0.66	0.058	0.71
"	"	336439	0.049	1.61	0.025	0.01	0.64	17.69	9.16	0.63	0.049	0.67
"	"	336440	0.05	0.92	0.026	0.013	0.58	17.92	9.66	0.67	0.047	0.717
"	"	336441	0.044	1.07	0.029	0.013	0.57	17.92	9.66	0.81	0.045	0.855

Table 5. Weld Procedure Certification for Repair Welds of the LOX Run Tank

Weld Procedure Certification No. G-4274 # 1: 1-17-65
Base Metal: SA-240-T347
Standards: Military Specification MIL E-22200 2A
Electrode: E308 ELC-16
250°F max interpass temp. Temperature to be checked by temple sticks ½" from area where weld bead is deposited. All weld slag will be completely removed before subsequent layers are deposited. All defects will be ground out to sound metal. Inspection: after gouging and grinding to the root of the outside weld, the groove preparation ½" on each side of the groove will be dye penetrant inspected. Dye penetrant inspection will be required at approx. 1 ½" of weld, 3" of weld and final welded joint. This procedure is applicable to the repair welding of the shell penetrations for approx. 4 ½" thick LOX storage tank.

1/8"	145	26
5/32"	165	26

Table 6. Summary of Crack Growth Analyses

Analysis	Initial Crack Size (inches)	Fracture Toughness, K_{IC} (ksi $in^{1/2}$)	Repair Residual Stress (ksi)	Cycles to Failure
Dye Penetrant Crack	0.1	83	35	131,923
Repair Crack	0.5	83	35	44,721
Flow stress repair resid.	0.5	83	62.5	20,647
Low Fracture toughness welds	0.5	40	35	0
	0.5	50	35	9,764
	0.5	60	35	23,748
	0.5	70	35	35,396

REPORT DOCUMENTATION PAGE

Form Approved
OMB No. 0704-0188

1. REPORT DATE *(DD-MM-YYYY)*	2. REPORT TYPE	3. DATES COVERED *(From - To)*
01- 02 - 2006	Technical Memorandum	

4. TITLE AND SUBTITLE

Damage Tolerance Analysis of a Pressurized Liquid Oxygen Tank

5a. CONTRACT NUMBER

5b. GRANT NUMBER

5c. PROGRAM ELEMENT NUMBER

6. AUTHOR(S)

Forth, Scott C.; Harvin, Stephen F.; Gregory, Peyton B.; Thompson, Jon E.; and Hoffman, Eric K.

5d. PROJECT NUMBER

5e. TASK NUMBER

5f. WORK UNIT NUMBER

732759.07.11

7. PERFORMING ORGANIZATION NAME(S) AND ADDRESS(ES)

NASA Langley Research Center
Hampton, VA 23681-2199

8. PERFORMING ORGANIZATION REPORT NUMBER

L-19212

9. SPONSORING/MONITORING AGENCY NAME(S) AND ADDRESS(ES)

National Aeronautics and Space Administration
Washington, DC 20546-0001

10. SPONSOR/MONITOR'S ACRONYM(S)

NASA

11. SPONSOR/MONITOR'S REPORT NUMBER(S)

NASA/TM-2006-214274

12. DISTRIBUTION/AVAILABILITY STATEMENT

Unclassified - Unlimited
Subject Category 39
Availability: NASA CASI (301) 621-0390

13. SUPPLEMENTARY NOTES

An electronic version can be found at http://ntrs.nasa.gov

14. ABSTRACT

A damage tolerance assessment was conducted of an 8,000 gallon pressurized Liquid Oxygen (LOX) tank. The LOX tank is constructed of a stainless steel pressure vessel enclosed by a thermal-insulating vacuum jacket. The vessel is pressurized to 2,250 psi with gaseous nitrogen resulting in both thermal and pressure stresses on the tank wall. Finite element analyses were performed on the tank to characterize the stresses from operation. Engineering material data was found from both the construction of the tank and the technical literature. An initial damage state was assumed based on records of a nondestructive inspection performed on the tank. The damage tolerance analyses were conducted using the NASGRO computer code. This paper contains the assumptions, and justifications, made for the input parameters to the damage tolerance analyses and the results of the damage tolerance analyses with a discussion on the operational safety of the LOX tank.

15. SUBJECT TERMS

Analysis; Damage; Liquid; Oxygen; Pressurized; Tank; Tolerance

16. SECURITY CLASSIFICATION OF:			17. LIMITATION OF ABSTRACT	18. NUMBER OF PAGES	19a. NAME OF RESPONSIBLE PERSON
a. REPORT	b. ABSTRACT	c. THIS PAGE			STI Help Desk (email: help@sti.nasa.gov)
					19b. TELEPHONE NUMBER *(Include area code)*
U	U	U	UU	36	(301) 621-0390